UC Santa Barbara

UC Santa Barbara Previously Published Works

Title

Atomically Precise Nanoclusters of Iron, Cobalt, and Nickel: Why Are They So Rare?

Permalink

https://escholarship.org/uc/item/9266j6q2

Author

Hayton, Trevor

Publication Date

2026-11-06

Copyright Information

This work is made available under the terms of a Creative Commons Attribution-NonCommercial License, available at https://creativecommons.org/licenses/by-nc/4.0/

eScholarship.org Powered by the California Digital Library
University of California

Chapter xx
Atomically Precise Nanoclusters of Iron, Cobalt, and Nickel: Why are They So Rare?

Trevor W. Hayton[*]

Department of Chemistry and Biochemistry, University of California Santa Barbara, Santa Barbara CA 93106, United States

Table of Contents:

x.1 Introduction

x.2 General Considerations

x.3 Synthesis of Ni APNCs

x.4 Synthesis of Co APNCs

x.5 Attempted Synthesis of Fe APNCs

x.6 Conclusion and Outlook

x.1 Introduction

Atomically Precise Nanoclusters (APNCs) are an emerging class of materials that feature properties common to both traditional metal complexes and bulk metals.[1] Their unique mix of properties make them attractive for a variety of applications,[2] including solid-state memory,[3] catalysis,[4-6] sensing,[7] and imaging.[7-8] Nanoclusters can also feature single molecule magnet (SMM) behavior,[9] and have been proposed to function as novel spin qubits.[10-12]

While a wide variety of APNC definitions are found in the literature, there are three requirements that are commonly agreed upon, namely, that APNCs must be monodisperse, nano-sized, and feature a well-

defined arrangement of their capping ligands.[13-14] For the purposes of this review, we will include a fourth requirement. Specifically, an APNCs must feature at least one metal atom that is bound to at least eight other metal atoms and no non-metal atoms. This criterion is met by those APNCs that feature an [M_{13}] kernel, such as the iconic Au_{25} APNC, [$NOct_4$][$Au_{25}(SCH_2CH_2Ph)_{18}$], which features a central gold atom that is bound to 12 other gold atoms in an icosahedral geometry, but no ligand atoms (Figure x-1).[15][16] However, other kernels also meet this criterion, including the [M_9] cubic kernel and the [M_{11}] sphenocorona kernel.[17-18] Importantly, this requirement restricts our discussion to APNCs that feature considerable amounts of metal–metal bonding and low average metal oxidation states (approaching zero in many cases). Put differently, these APNCs feature "metal-like" character. APNCs made of transition metal oxides, chalcogenides, or pnictinides are not included within this definition and so will not be discussed. APNCs with interstitial carbide and hydride ligands are also not included. Additionally, for convenience, we will restrict our discussion to homometallic APNCs.

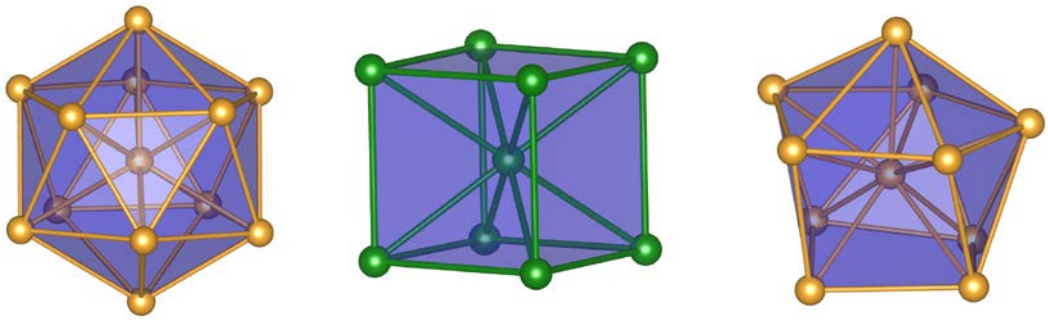

Figure x-1. The [M_{13}], [M_9], and [M_{11}] kernels found in [$NOct_4$][$Au_{25}(SCH_2CH_2Ph)_{18}$], [$Ni_9Te_6(PEt_3)_8$], and [$Au_{11}Cl_3(PR_3)_7$] (R = 3-$CF_3C_6H_4$), respectively. Data taken from Refs. [15, 17-18].

Finally, we will restrict our discussion to APNCs containing nickel, cobalt, and iron. This restriction was implemented because APNCs of these metals have not been widely reviewed. APNC reviews tend to focus on the group 11 metals,[2, 19-21] and do not focus much attention on the mid transition metals. This emphasis makes sense, given that most APNCs contain one of the coinage metals and given that APNCs of nickel, cobalt, and iron are exceptionally rare (for reasons that should become apparent in following sections). However, the emphasis placed on the group 11 APNCs means that the interesting properties of nickel, cobalt, and iron APNCs are often underappreciated. In particular, APNCs of these metals are

reasonably expected to be open shell, in contrast to group 11 APNCs. Open shell APNCs are generally rare, and their magnetic properties are not well understood. However, preliminary evidence suggests that low-valent, open shell APNCs of Fe, Co, and Ni should be good single molecule magnets (SMMs),[22] as evidenced by the SMM behavior of the small cluster complexes, $[NBu_4][(^{H}L)_2Fe_6(py)_2]$ ($^{H}LH_6$ = $MeC(CH_2NHPh\text{-}o\text{-}NH_2)_3$)[23] and $[Co_4(N=P^tBu_3)_4][B(C_6F_5)_4]$ (Figure x-2).[24-25] Persistent molecular magnetism requires the presence of a barrier (U) to magnetic reversal. The larger the barrier, in principle, the better the performance. In integer spin systems, U is directly correlated to spin state (S) and the zero field splitting (D) according to $U = |D|S^2$.[26] Thus, the ability of $[(^{H}L)_2Fe_6(py)_2]^-$ (S = 11) and $[Co_4(N=P^tBu_3)_4]^+$ (S = 9/2) to function as SMMs relates partly to their large spin ground states, which are a consequence of the direct metal-metal bonding interactions that are found in their structures. This metal-metal bonding promotes ferromagnetic coupling of the unpaired spins via the "Direct exchange" mechanism.[24] Importantly, this relationship suggests that higher nuclearity metal-metal bonded APNCs with larger spin ground states should possess even better SMM performance.

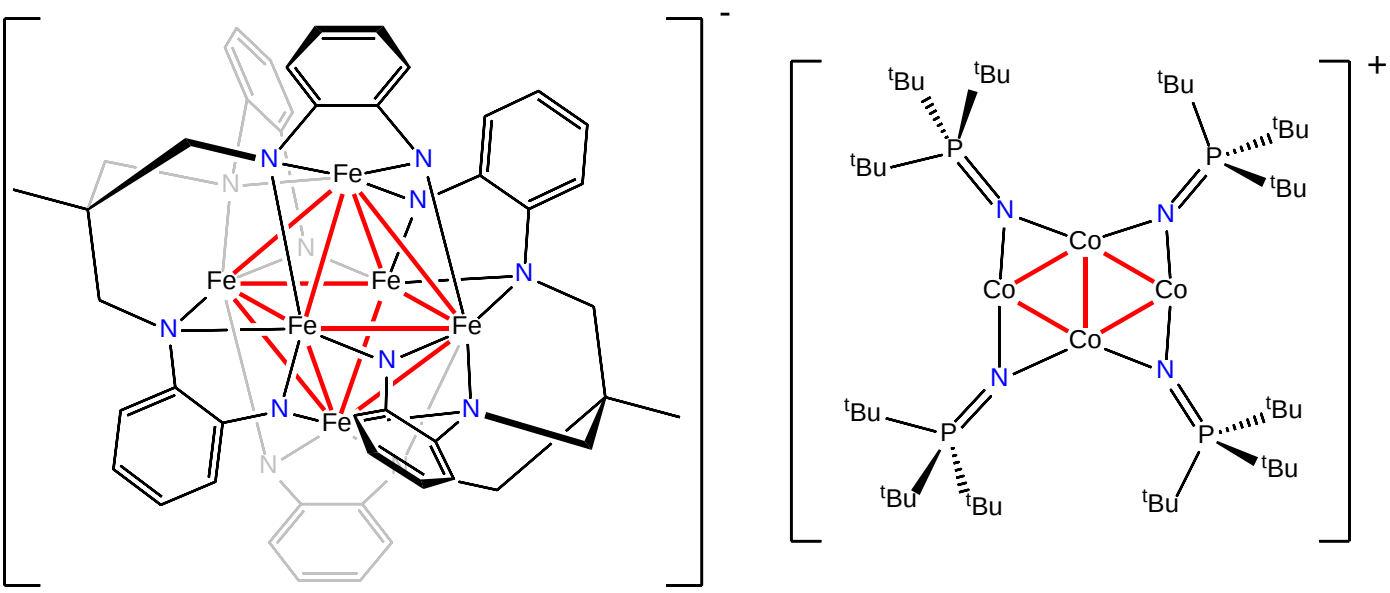

Figure x-2. Molecular structures of $[(^{H}L)_2Fe_6(py)_2]^-$ and $[Co_4(N=P^tBu_3)_4]^+$. Direct exchange interactions are shown in red.

In this chapter, we will attempt to identify the reasons for the paucity of Fe, Co, and Ni APNCs and highlight potential synthetic strategies for accessing APNCs of these metals. In addition, we will discuss the

unique properties of these open-shell APNCs. We hope that a discussion of these topics will accelerate the discovery of these uncommon materials.

x.2 General Considerations

As mentioned above, there are very few examples of homometallic Fe, Co, and Ni clusters that meet our definition of an APNC. Indeed, a search of the Cambridge Structural Database (CSD) reveals that there are zero, three, and nine structurally-characterized homometallic APNCs of these metals, respectively (Table x-1). In contrast, APNCs of silver and gold are quite common. Indeed, there are now 194 structurally characterized homometallic Au APNCs, many of which have been made in the past 5 years, which reflects the excitement surrounding this field.

To understand this disparity, it is useful to examine the reduction potentials as well as the diatomic M-M bond dissociation enthalpies (BDEs) for the relevant transition metal ions (Table x-1). For instance, the BDE for gas phase Au_2 is 226 kJ/mol, whereas the BDEs for gas phase Fe_2 and Co_2 are 118 and <127 kJ/mol, respectively. Thus, it appears that Au APNCs are so abundant, in part, because the strong Au-Au bonds can successfully drive APNC self-assembly.[19] A comparison of the metal reduction potentials is also informative. The standard $Au^{+1/0}$ reduction potential is +1.69 V, whereas the standard $M^{+2/0}$ reduction potentials for Fe and Co are -0.44 and -0.28 V, respectively (Table x-1). Thus, it is much easier reduce an Au(I) starting material to Au(0) than to reduce a Fe(II) or Co(II) starting material to the zero-valent state. Indeed, many attempted APNC syntheses are unsuccessful because the reducing agents employed are not strong enough to reduce the metal salts to M(0).[27-28] Additionally, for elements with large reduction potentials, it can be a challenged to keep an APNC in a low-valent state once it is formed. These APNCs are easily oxidized by O_2, necessitating the use of inert atmosphere techniques during their isolation and characterization. These strongly reducing metal atoms can also reduce many common stabilizing ligands, such as thiolates and phosphines, and several examples of this phenomenon will be discussed in the sections below. Accordingly, their isolation necessitates the use of carefully designed, redox-stable ligands.

The analysis described above has its limitations, however. For example, no homometallic APNCs are known for Os or Ir, despite their apparently favorable M-M BDEs and reduction potentials. In these two

examples, it may be that the paucity of examples is due to the relatively high cost of the elements, which has perhaps limited the amount of research that has been performed on these metals. The case of Ru is more challenging to explain. It has a favorable M-M BDE (190 kJ/mol), a favorable reduction potential (+0.8 V), and is relatively cheap, but no APNCs have been reported for this metal, suggesting that the factors affecting APNC formation are more complex than suggested by this analysis. Nickel also has an apparently favorable M-M BDE of 204 kJ/mol, which is similar to that of Au. However, only a handful of Ni APNCs have ever been isolated. In this particular case, though, Ni displays an unfavorable $M^{+2/0}$ reduction potential (-0.24 V), in line with those of Fe and Co.

Table x-1. Number of Structurally Characterized APNCs, M-M Bond Strengths, and Standard Redox Potentials for Selected Transition Metal Ions

Group	**M**	**M-M BDE (kJ/mol)[a]**	**E° (V, vs. SHE)[b]**	***n***	**Number of examples[c]**
8	Fe	118	-0.44	2	0
	Ru	190	+0.8	2	0
	Os	420	+0.9	3	0
9	Co	<127	-0.28	2	3
	Rh	234	+0.76	3	11
	Ir	360	+1.0	3	0
10	Ni	204	-0.24	2	9
	Pd	>136	+0.915	2	24
	Pt	306	+1.18	2	13
11	Cu	201	+0.52	1	10
	Ag	162	+0.80	1	47
	Au	226	+1.69	1	194

a. Values correspond to experimentally measured gas phase BDEs for the neutral diatomic species. Data taken from Ref. [29]. While the M-M bond strengths in an APNCs will be different, values for the diatomic species were chosen for comparison because they are experimentally known for a wide variety of metals.

b. Standard Redox Potentials for the $M^{n+}(aq) + ne^- \rightarrow M(s)$ Couple. Data taken from Ref. [30].

c. Data taken from a search of the Cambridge Structural Database (CSD), Version 5.42 (September 2021 update). Defined here as a cluster that contains at least one transition metal atom coordinated to at least eight other transition metal atoms and no non-metal atoms. The search was restricted to homometallic APNCs.

x.3 Synthesis of Ni APNCs

The earliest attempts to form large metal clusters focused on the use of carbon monoxide as the supporting ligand.[31-32] Indeed, within group 10, several large homoleptic carbonyl-supported APNCs have been reported over the years, including $[Pd_{66}(CO)_{45}(PEt_3)_{16}]$ and $[Pt_{38}(CO)_{44}]^{2-}$,[33-34] but these very large clusters are restricted to Pd and Pt. Homoleptic Ni carbonyl clusters are known, including $[Ni_6(CO)_{12}]^{2-}$, $[Ni_9(CO)_{l8}]^{2-}$, and $[Ni_{l2}(CO)_{21}]^{4-}$,[35-36] but they tend to be much smaller, at least relative to known homoleptic Pd and Pt carbonyl clusters.[34, 37-39] In the case of Ni, cluster growth is typically achieved by addition of $[Ni(CO)_4]$ to a low nuclearity Ni carbonyl precursor. For example, $[Ni_9(CO)_{l8}]^{2-}$ can be prepared by addition of 3 equiv of $Ni(CO)_4$ to $[Ni_6(CO)_{12}]^{2-}$.[32] The largest homoleptic Ni carbonyl cluster appears to be the aforementioned $[Ni_{l2}(CO)_{21}]^{4-}$, along with its protonated analogues, $[Ni_{12}(CO)_{21}H_{4-n}]^{n-}$ (n = 2, 3).[40-41] The structure of D_{3h}-symmetric $[Me_4N]_3[Ni_{l2}(CO)_{21}H]$ consists of a planar $[Ni_6(CO)_3(\mu\text{-}CO)_6]$ fragment sandwiched by two planar $[Ni_3(CO)_3(\mu\text{-}CO)_3]$ fragments (Figure x-3).[42] As a result of this arrangement, every Ni atom is bound by at least two CO ligands. Larger clusters are possible, but they feature interstitial main group atoms, such as carbon, in their structures. Examples include $[HNi_{38}(CO)_6(\mu\text{-}CO)_{36}C_6]^{5-}$ and $[Ni_{32}C_6(CO)_{36}]^{6-}$.[43-44] Because of the presence of interstitial main group atoms, these clusters to not obey our definition of an APNC and will not be discussed in detail. Presumably, larger homoleptic carbonyl clusters cannot be made because any structure with n > 12 would require an interstitial Ni atom (assuming formation of a cuboctahedral kernel), which is evidently unfavorable because Ni(0) is so reducing.

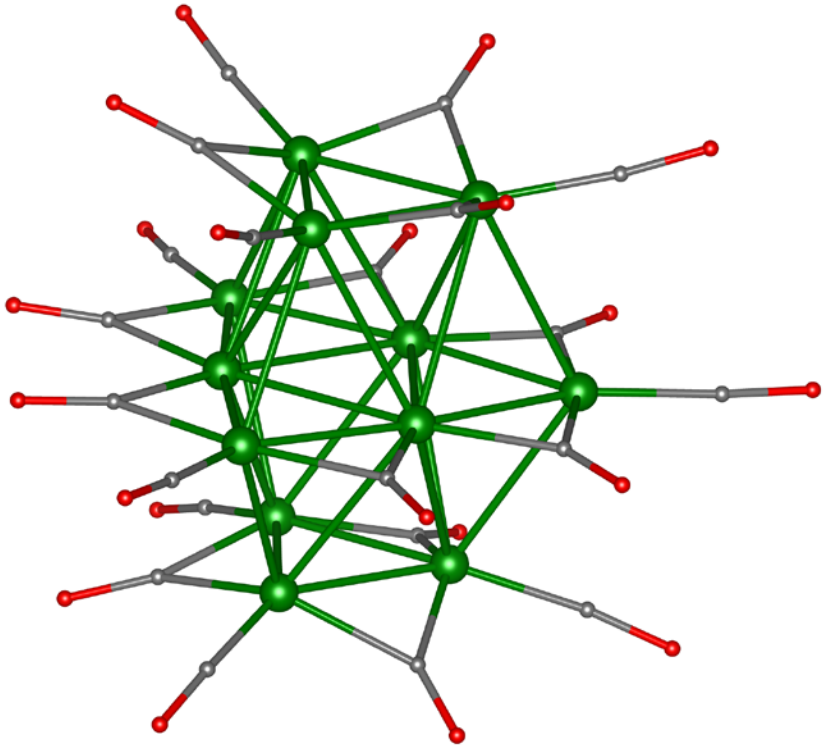

Figure x-3. Solid-state structure of $[Me_4N]_3[Ni_{12}(CO)_{21}H]$. Ni, C, and O atoms are shown in green, grey, and red, respectively. Hydrogen atom and $[Me_4N]^+$ counterions are omitted for clarity. Data taken from Ref [42].

A number of large carbonyl clusters have been reported that contain mixtures of Ni with other metals, including Pd, Pt, and Au. Their structures are also informative. For example, $[Pt_6Ni_{38}(CO)_{48}H_{6-n}]^{n-}$ (n = 3, 4, 5, 6) features an octahedral $[Pt_6]$ kernel surrounded by a shell of 38 Ni atoms.[45-47] Each Ni atom is further bound by a mix of terminal and bridging CO ligands. The partitioning of the Pt atoms within the core is consistent with the greater redox stability of Pt(0) vs. Ni(0) (Table x-1). Stated differently, the more strongly reducing Ni(0) prefers to be bound by the strongly π-accepting CO ligands, which ameliorates its high reducing power. A similar picture emerges for other mixed-metal group 10 clusters,[48-50] including $[Pd_{33}Ni_9(CO)_{41}(PPh_3)_6]^{4-}$,[51] $[Au_6Ni_{32}(CO)_{44}]^{6-}$,[52] $[Ni_{29}Pd_6(CO)_{42}]^{6-}$,[53] and $[HNi_{24}Pt_{17}(CO)_{25}(CO)_{21}]^{5-}$.[54] In all of these examples, and despite the presence of substitutional disorder in some cases, every Ni atom resides on the cluster surface.

While the synthesis of Ni APNCs via $Ni(CO)_4$ condensation has been unsuccessful thus far, a handful of Ni APNCs have been made via different routes,[55] including $[Ni_{23}Se_{12}Cl_3(PEt_3)_{10}]$, $[Ni_{21}Se_{14}(PEt_2Ph)_{12}]$,[56] and $[Ni_9Te_6(PEt_3)_8]$.[17] For example, we recently prepared $[Ni_{23}Se_{12}Cl_3(PEt_3)_{10}]$ via reaction of [Ni(1,5-COD)$_2$] (1.0 equiv), PEt_3 (0.04 equiv), $SePEt_3$ (0.52 equiv), and $[NiCl_2(PEt_3)_2]$ (0.07 equiv), in a mixture of

toluene and THF.[57] It can be isolated in 35% yield when prepared via this route. Interestingly, this cluster was first synthesized in 1992 by Steigerwald and co-workers;[58] however, it was originally formulated as $[Ni_{23}Se_{12}(PEt_3)_{13}]$ on the basis of an incomplete X-ray crystallographic analysis. In the solid-state, $[Ni_{23}Se_{12}Cl_3(PEt_3)_{10}]$ features a central $[Ni_{13}]$ anti-cuboctahedral kernel, making it only one of two Ni APNCs to contain this structural feature (Figure x-4). One hemisphere of the $[Ni_{13}]$ kernel is encapsulated by a $[Ni_{10}(\mu\text{-}Se)_9Cl_3(PEt_3)_7]^-$ shell, whereas the other hemisphere is ligated by three $(\mu_4\text{-}Se)^{2-}$ ligands and three PEt_3 ligands. Within the $[Ni_{13}]$ cuboctahedron, the average $Ni_{central}$-Ni_{shell} distance is 2.54 Å (range = 2.516(4) - 2.578(6) Å), which is somewhat longer than the Ni-Ni distance in bulk fcc Ni (2.48 Å).[59] Evans method magnetism measurements suggest that $[Ni_{23}Se_{12}Cl_3(PEt_3)_{10}]$ has three unpaired electrons.

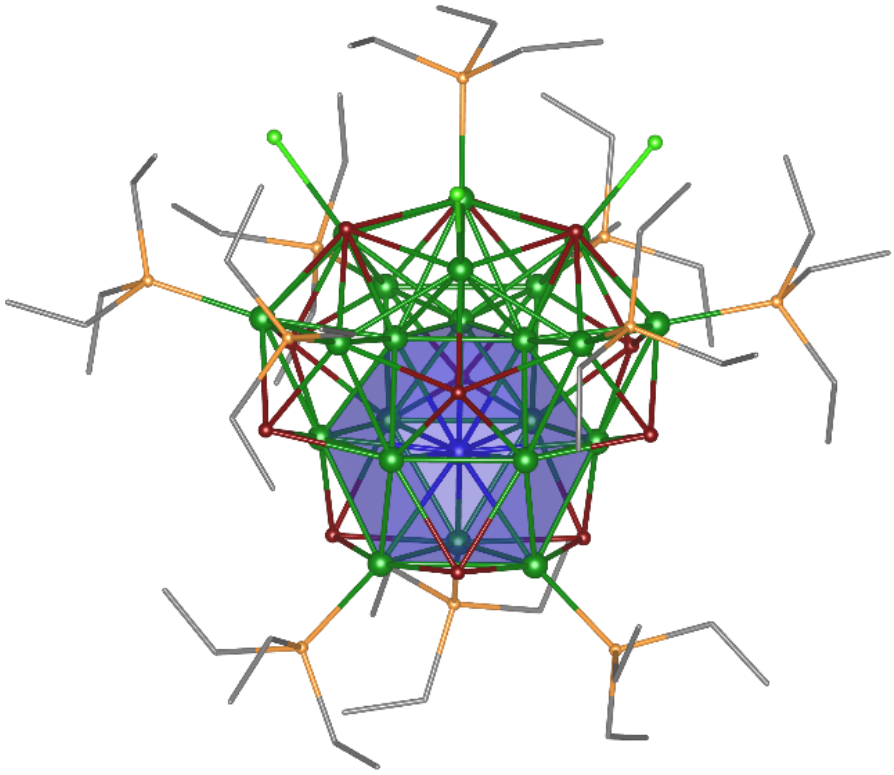

Figure x-4. Solid-state structure of $[Ni_{23}Se_{12}Cl_3(PEt_3)_{10}]$. Ni atoms are shown in green, except for the central Ni atom, which is shown in blue. The blue polyhedron represents the coordination sphere of the central Ni atom. P, Se, and Cl atoms are shown in saffron, maroon, and bright green, respectively. C atoms are depicted in grey wireframe. Hydrogen atoms and THF solvate atoms are omitted for clarity. Data taken from Ref. [57]

In 1992, Fenske and co-workers reported the synthesis of $[Ni_{21}Se_{14}(PEt_2Ph)_{12}]$, which can be prepared by reaction of $[NiCl_2(PEt_2Ph)_2]$ with $Se(SiMe_3)_2$ over the course of two weeks at room temperature, followed by crystallization from heptane.[56] A yield was not reported for this cluster. The average Ni oxidation state

is +1.33. The reducing agent required to convert the Ni(II) starting material to the reduced APNC product is most likely PEt_2Ph, as $SePEt_2Ph$ is formed as a by-product in the reaction. Me_3SiCl is also a by-product of the transformation. The use of an Ni(II) starting material here is notable, as other Ni APNC syntheses that started from Ni(II) precursors fail to achieve any metal reduction (see below for further discussion). $[Ni_{21}Se_{14}(PEt_2Ph)_{12}]$ features a central $[Ni_{13}]$ cuboctahedral kernel, which is capped by two $[Ni_4(\mu_4\text{-}Se)_5(PEt_2Ph)_4]$ terraces that are found at the north and south poles (Figure x-5). Additionally, there are four $(\mu_4\text{-}Se)^{2-}$ ligands and four PEt_2Ph ligands located along the equatorial belt of the $[Ni_{13}]$ cuboctahedron. Within the $[Ni_{13}]$ cuboctahedron, the $Ni_{central}$-Ni_{shell} distances range from 2.576 to 2.800 Å, whereas the Ni_{shell}-Ni_{shell} distances range from 2.606 to 2.724 Å. Similar values were observed for $[Ni_{23}Se_{12}Cl_3(PEt_3)_{10}]$. The magnetic properties of $[Ni_{21}Se_{14}(PEt_2Ph)_{12}]$ were not mentioned in the original report; however, they would be of interest for comparison to those of $[Ni_{23}Se_{12}Cl_3(PEt_3)_{10}]$ and $[Ni_9Te_6(PEt_3)_8]$. Because of these unknowns, coupled with the overall rarity of Ni APNCs, this cluster is a candidate for further study.

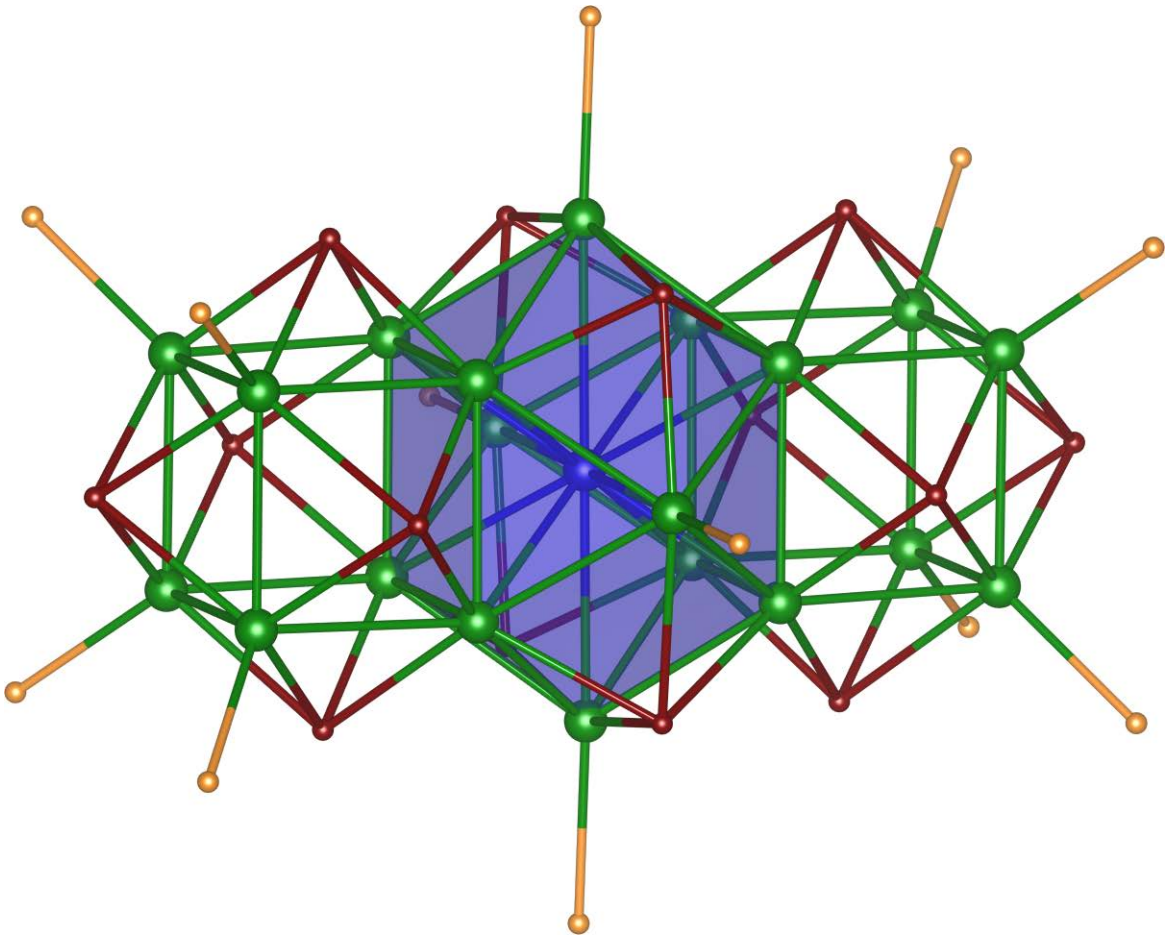

Figure x-5. Solid-state structure of $[Ni_{21}Se_{14}(PEt_2Ph)_{12}]$. Ni atoms are shown in green, except for the central Ni atom, which is shown in blue. The blue polyhedron represents the coordination sphere of the central Ni atom. P and Se atoms

are shown in saffron and maroon, respectively. Carbon and hydrogen atoms are omitted for clarity. Data taken from Ref. [56]

Reaction of $[Ni(1,5\text{-}COD)_2]$ with Et_3PTe and Et_3P in a 2:1:22 ratio leads to formation of $[Ni_9Te_6(PEt_3)_8]$ in 45% yield.[17, 60] This cluster features an $[Ni_9]$ nickel-centered cubic kernel that is encapsulated by six $(\mu_4\text{-}Se)^{2-}$ ligands arranged on the square faces of the cube (Figure x-6). Additionally, the eight outer Ni atoms are each bound by a PEt_3 ligand. The average $Ni_{central}$-Ni_{shell} bond length is 2.47 Å, whereas average Ni_{shell}-Ni_{shell} distance is 2.85 Å. The average $Ni_{central}$-Te bond length is 2.98 Å, suggesting that there is no meaningful $Ni_{central}$-Te interaction. As a result, $[Ni_9Te_6(PEt_3)_8]$ qualifies as an APNC by our definition. $[Ni_9Te_6(PEt_3)_8]$ exhibits a room temperature magnetic moment of 4.9 μ_B, which corresponds to an $S = 2$ spin state.[61-62] Electronic structure calculations performed by Saillard and co-workers suggest a ground state configuration of $(e_g)^4(t_{1g})^4(t_{2g})^2$, which is consistent with the magnetism measurements.[63-64] Additionally, they found that the Ni-Ni bonds within the Ni_8 cage are derived primarily from 4s and 4p atomic orbitals, while the central Ni atom interacts with the cage via its 4s and 4p orbitals. The 3d subshell of the central Ni atom is fully filled. Earlier calculations by Wheeler uncovered a similar bonding picture.[65-66] Calculations have also been performed on the CO-substituted analogue, $[Ni_9Te_6(CO)_8]$.[67] Magnetic measurements on $[Ni_9Te_6(PEt_3)_8][BF_4]$ and $[Ni_9Te_6(PEt_3)_8][BF_4]_2$ have also been reported;[61-62] although no synthetic or structural details were provided. $[Ni_9Te_6(PEt_3)_8][BF_4]$ and $[Ni_9Te_6(PEt_3)_8][BF_4]_2$ feature moments of 3.7 and 1.9 μ_B at room temperature, respectively, which are both lower than the moment observed for the neutral cluster, as expected.

$[Ni_9Te_6(PEt_3)_8]$ reacts with C_{60} to form $[Ni_9Te_6(PEt_3)_8][C_{60}]$, a material with a NaCl-type lattice.[68] This material exhibits ferromagnetic ordering below 4K in the solid-state. X-ray crystallography reveals that the Ni-Ni and Ni-Te distances within the $[Ni_9Te_6(PEt_3)_8]^+$ cation are essentially identical to those of the neutral cluster. The closely related analogues, $[Ni_9Te_6(PMe_3)_8][C_{60}]$ and $[Ni_9Te_6(PEt_3)_8][C_{70}]$ have also been reported.[69]

Several clusters with closely related $[Ni_9]$ kernels are also known,[70] including $[Ni_9(GeEt)_6(CO)_8]$,[71] $[Ni_9(As)_6(PPh_3)_5Cl_3]$,[72] $[Ni_9(As)_6(PPh_3)_6Cl_2]$,[72] and $[Ni_9(\mu_4\text{-}P)_6(PCy_3)_6Cl_2]$.[73] Generally, these clusters are synthesized by reaction of $[NiCl_2(PR_3)_2]$ with $E(SiMe_3)_3$ or $PhE(SiMe_3)_2$ (E = main group

element).[72-73] However, $[Ni_9(GeEt)_6(CO)_8]$ is formed by reaction of $[Ni_6(CO)_{12}]^{2-}$ with $EtGeCl_3$.[71] In $[Ni_9(As)_6(PPh_3)_5Cl_3]$, the average Ni_{center}-As distance is 2.61 Å,[72] whereas in $[Ni_9(\mu_4\text{-}P)_6(PCy_3)_6Cl_2]$, the average Ni_{center}-P distance is 2.44 Å.[73] These distances lie just outside of their respective single bond covalent radii,[74] suggesting that these clusters also fit our definition of an APNC. Nonetheless, there may still be weak Ni_{center}-E interactions in these materials.

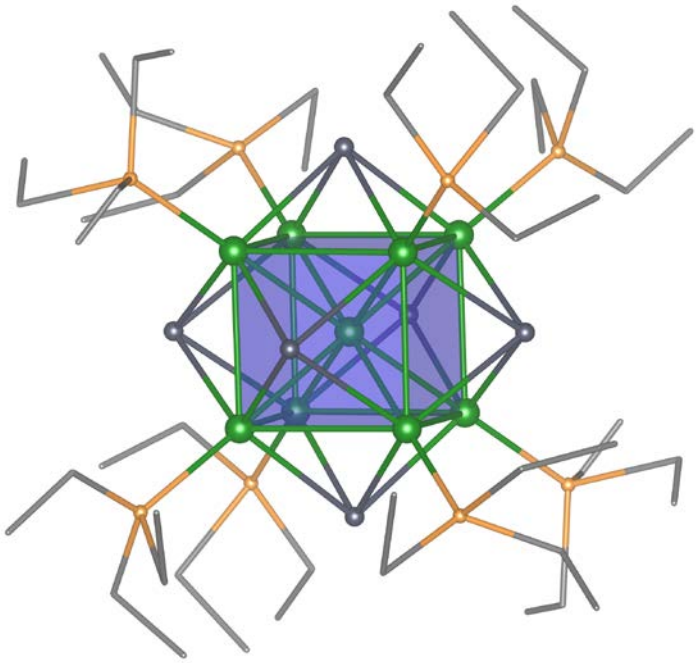

Figure x-6. Solid-state structure of $[Ni_9Te_6(PEt_3)_8]$. Ni, P, and Te atoms are shown in green, orange, and silver, respectively. The blue polyhedron defines the coordination sphere of the central Ni atom. Carbon atoms are shown in wireframe and hydrogen atoms are omitted for clarity. Data taken from Ref. [17]

No other Ni clusters with $[M_{13}]$ or $[M_9]$ kernels are known; however, a number Ni clusters with mixed-element $[Ni_{11}E_2]$ icosahedral kernels have been reported. While these clusters do not fall within the definition of APNCs used in this chapter, as defined in Section x.1, their synthesis, structure, and bonding are highly informative. For example, in 1992, Dahl and co-workers reported the synthesis of $[PPh_3Me]_2[Ni_{11}Se_2(CO)_{18}]$ via reaction of PhSeCl with $[PPh_3Me]_2[Ni_6(CO)_{12}]$.[75] Also formed in the reaction is $NiCl_2$ and $Ni(CO)_4$. The selenium source for this transformation, PhSeCl, presumably undergoes a C-Se oxidative addition during the reaction, losing its phenyl group as biphenyl. A similar sequence of reaction steps has been reported for the synthesis of $[Ni_8(S)_5(PPh_3)_7]$ from PhSSPh and $[Ni(1,5\text{-}COD)_2]$.[76] In the solid state, $[PPh_3Me]_2[Ni_{11}Se_2(CO)_{18}]$ features a $[Ni_{11}Se_2]$ Ni-centered icosahedron, wherein the two

(μ_5-Se)$^{2-}$ ligands are found at the north and south poles (Figure X-7). Additionally, each outer Ni atom is bound by a terminal CO ligand, and there are eight μ-CO ligands arranged along the equatorial belt. The $Ni_{central}$-Se distance is 2.19 Å, the average $Ni_{central}$-Ni_{shell} bond length is 2.55 Å, and the average intra- and inter-pentagonal Ni_{shell}-Ni_{shell} distances are 2.74 and 2.52 Å, respectively. The central Ni atom is thought to feature a d^{10} electronic configuration. A bonding analysis of the closely-related cluster, $[Ni_{10}Sb_2(\mu_{12}\text{-}Ni)\{Ni(CO)_3\}_2(CO)_{18}]^{2-}$ suggests that the 3d orbitals of the interstitial Ni(0) atom do not interact very strongly with the cage atoms.[77-78] Moreover, reducing this cluster by one electron to form $[Ni_{10}Sb_2(\mu_{12}\text{-}Ni)\{Ni(CO)_3\}_2(CO)_{18}]^{3-}$ does not change the M-M bond lengths, suggesting that the extra electron occupies a non-bonding or slightly antibonding orbital within $[Ni_{11}Sb_2]$ core.[77] Magnetism measurements of $[EtV]_8[Ni_{10}Sb_2(\mu_{12}\text{-}Ni)\{Ni(CO)_3\}_2(CO)_{18}]_3$ (EtV = 1,1′-diethyl-4,4′-bipyridilium cation), which features two open-shell $[Ni_{10}Sb_2(\mu_{12}\text{-}Ni)\{Ni(CO)_3\}_2(CO)_{18}]^{3-}$ trianions and one closed-shell $[Ni_{10}Sb_2(\mu_{12}\text{-}Ni)\{Ni(CO)_3\}_2(CO)_{18}]^{2-}$ dianion, are consistent with an $S = 1$ ground state for the trianion.[79] Other clusters with the same $[Ni_{11}E_2]$ skeleton include $[Ni_{11}(SnR)_2(CO)_{18}]^{2-}$ (R = ^{n}Bu, Me)[70] and $[Ni_{11}Bi_2(CO)_{18}]^{n-}$ (n = 2 or 3).[80]

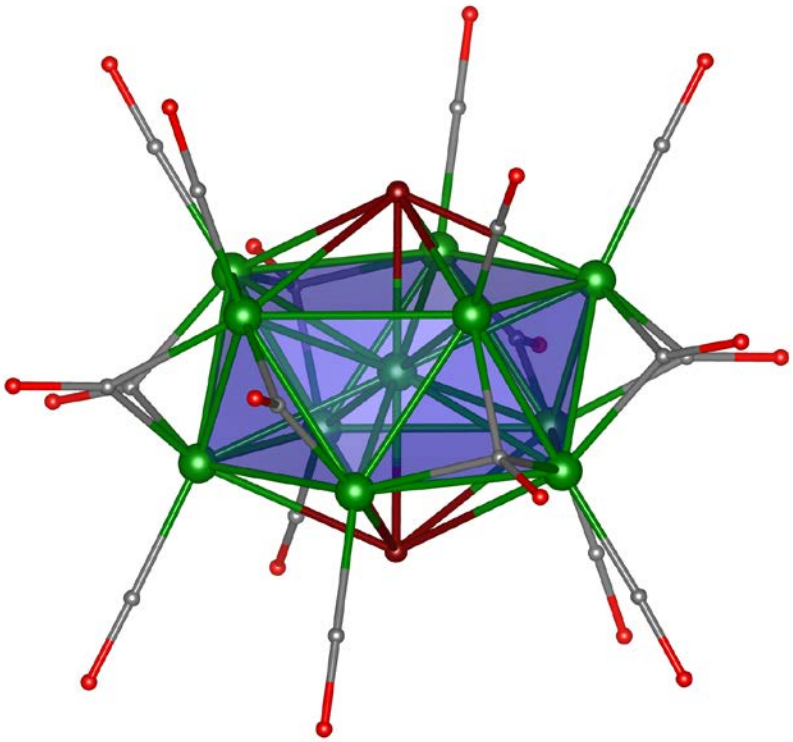

Figure x-7. Solid-state structure of $[PPh_3Me]_2[Ni_{11}Se_2(CO)_{18}]$. Ni, Se, C, and O atoms are shown in green, maroon, grey, and red, respectively. The blue polyhedron defines the ten Ni-Ni bonds from the central Ni atom. Counterions are omitted for clarity. Data taken from Ref. [75]

There have been many other attempts to prepare low-valent Ni APNCs, but all have been unsuccessful. For example, the reaction of reaction of $NiCl_2$ with $PhCH_2CH_2SH$ and excess $NaBH_4$, in the presence of $[NOct_4][Br]$, resulted in isolation of $[Ni_6(SCH_2CH_2Ph)_{12}]$, which adopts a "tiara-like" structure in the solid-state (Scheme x-1).[81-83] Importantly, every Ni atom in this cluster is in the 2+ oxidation state, demonstrating that, despite the use of Brust-Schiffrin reaction conditions, no metal ion reduction has occurred.[27] The contrast between this synthetic outcome and those involving the coinage metal triad, which readily undergo reduction using the Brust-Schiffrin protocol, can be explained by the much smaller reduction potential found for Ni^{2+} vs. the group 11 metals (Table x-1).

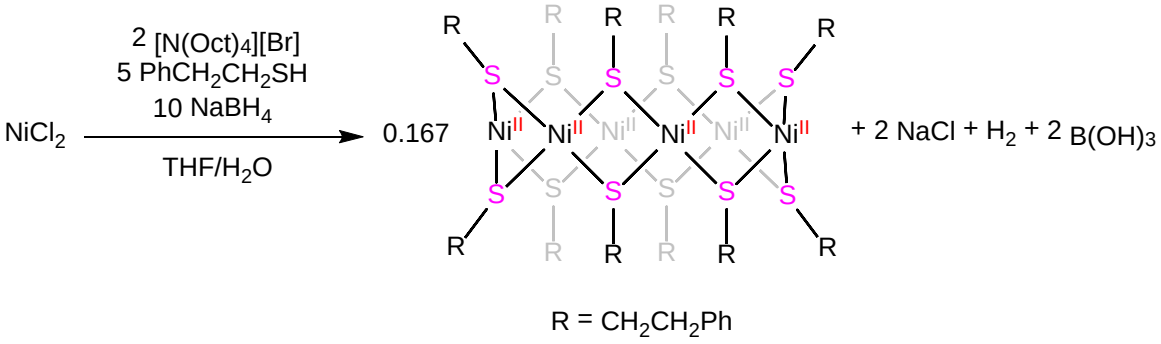

Scheme x-1. Synthesis of $[Ni_6(SCH_2CH_2Ph)_{12}]$

In an effort to circumvent the challenge of reducing Ni^{2+} *in situ* during APNC formation, several research groups have employed Ni(0) precursors to synthesize Ni APNCs. For example, reaction of bis(trityl)nickel, $Ni(\eta^3\text{-}CPh_3)_2$, which, on account of the high stability of the trityl radical, functions as a Ni(0) synthon due to the facile homolysis of the Ni-trityl bonds, with 2 equiv of PPh_3 at 75 °C in toluene results in formation of the phosphinidene cluster, $[Ni_3(\mu_3\text{-}PPh)(\mu\text{-}PPh_2)_2(PPh_3)_3]$ in moderate yield.[84] We hypothesize that the reaction proceeds through a $[Ni_2(\mu\text{-}PPh_2)_2(PPh_3)_3]$ intermediate. (Scheme x-2). Its phosphide ligands are formed by P-C oxidative addition, which is followed by C-C reductive elimination to form biphenyl. The phosphinidene ligand in $[Ni_3(\mu_3\text{-}PPh)(\mu\text{-}PPh_2)_2(PPh_3)_3]$ is formed similarly. This unwanted PPh_3 reduction thwarted attempts to make larger Ni APNCs via this route and nicely demonstrates how strongly reducing and reactive Ni(0) can be, when it is unencumbered by good π-accepting ligands, such as CO.

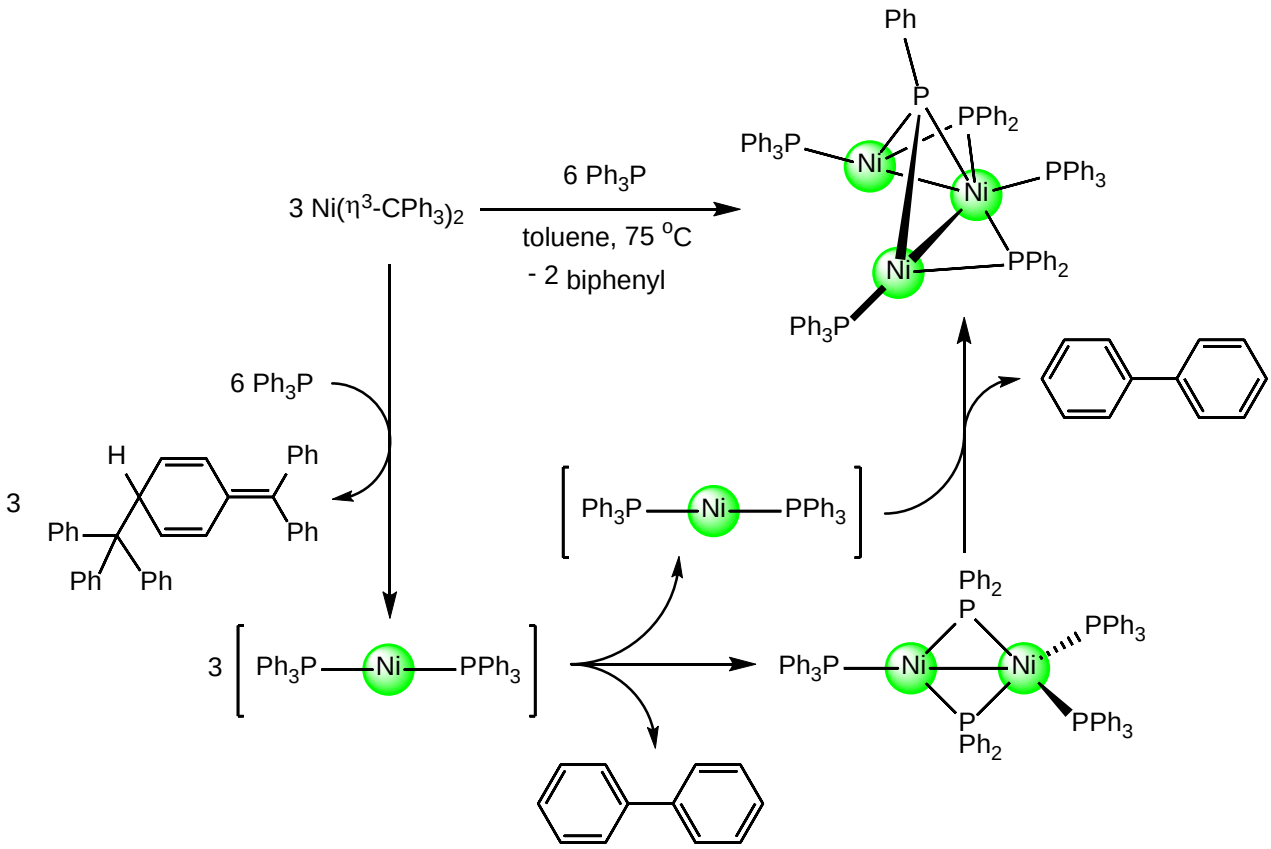

Scheme x-2. Proposed mechanism for formation of [$Ni_3(\mu_3$-PPh)(μ-$PPh_2)_2(PPh_3)_3$].

A similar phosphine activation is observed during the synthesis of Ni NPs.[85] Thermolysis of $Ni(acac)_2$ and $P(Oct)_3$ in a solution of di(octyl)ether/oleylamine at 230 °C for 1 h results in production of relatively monodisperse 22 nm Ni(0) nanoparticles. Powder X-ray diffraction shows that the Ni NPs possess an fcc Ni structure. However, ICP-OES and EXAFS experiments reveal 5 % incorporation of atomic P into the lattice. The structural data suggests that the P atoms are located at Ni sites and not at interstitial sites. Presumably, phosphorus incorporation occurs via a similar sequence of reaction steps observed in the formation of [$Ni_3(\mu_3$-PPh)(μ-$PPh_2)_2(PPh_3)_3$], namely, sequential P-C oxidative additions and C-C reductive eliminations, via $[PR_2]^-$ and $[PR]^{2-}$ intermediates. The phosphorus doping affects the magnetic properties of the NPs, but the structure is unchanged from the fcc lattice of Ni. Thus, if only a limited suite of characterization techniques (e.g., powder X-ray diffraction) is performed on the isolated material, the P doping could be missed. These results also suggest that element doping into transition metal nanoparticles may be common, especially for the highly reducing ferrous metals. Interestingly, tri-*n*-octylphosphine oxide (TOPO) can also be used purposefully as a P atom source, as in the case of the Co_2P nanocrystals reported by Robinson and co-workers.[86]

Further evidence for the high reducing ability of Ni(0) comes from the isolation of $[Ni_8(CN^tBu)_{12}][Cl]$, which could be prepared in low yield by reaction of $[Ni(1,5\text{-}COD)_2]$ with CN^tBu, followed by oxidation with adventitious $CHCl_3$.[87] Its formula suggests that the average Ni oxidation state is +0.125; however, the structural analysis suggests that this value is a gross simplification. In particular, this cluster features a folded nanosheet structure containing two symmetry-related planar Ni_4 arrays hinged about an Ni-Ni bond (Figure x-8). Six of the *tert*-butyl isocyanide ligands are terminally-bound, whereas six feature bridging $\mu\text{-}\eta^2\text{:}\eta^1$ binding modes. The metrical parameters of the bridging isocyanide ligands suggest that they are doubly reduced, i.e., they should be considered to be $[^tBuN{=}C]^{2-}$, which implies that Ni atoms along the outer edges of the nanosheet adopt the 2+ oxidation state. In contrast, the Ni atoms that form the hinge likely have an oxidation state of +0.5 each. This results demonstrates that, for isocyanide-stabilized Ni nanoclusters, a non-compact sheet structure is preferred over a compact spherical structure, despite the fact that isocyanide is a relatively good π-acceptor that should be able to support the formation of a spherical Ni(0) APNC.

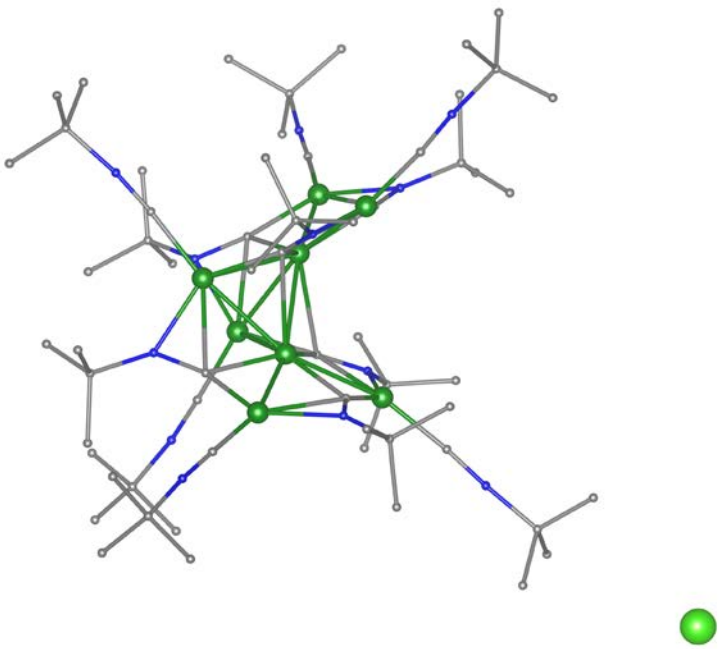

Figure x-8. Solid-state structure of $[Ni_8(CN^tBu)_{12}][Cl]$. Ni, N, Cl, and C atoms are shown in green, blue, grey, and bright green, respectively. Hydrogen atoms are omitted for clarity. Data taken from Ref. [87]

Another example that highlights the challenges inherent in making Ni(0)-containing APNCs comes the study of nanocluster growth within the $[Ni(1,5\text{-}COD)_2]$/PhSSPh/PEt_3 system.[76] Heating a combination of $[Ni(1,5\text{-}COD)_2]$, PhSSPh, and PEt_3 results in formation of $[Ni_8(S)_5(PEt_3)_7]$ via series of intermediate clusters,

including $[Ni_3(SPh)_4(PEt_3)_3]$, $[Ni_4(S)(Ph)(SPh)_3(PEt_3)_3]$, and $[Ni_5(S)_2(SPh)_2(PEt_3)_5]$ (Scheme x-3). Importantly, the isolation of the organometallic cluster $[Ni_4(S)(Ph)(SPh)_3(PEt_3)_3]$, coupled with the observation of biphenyl in the reaction mixture, demonstrates that S^{2-} incorporation into these clusters occurs via sequential C-S oxidative addition and C-C reductive elimination steps. A similar series of steps is likely responsible for Se^{2-} incorporation into $[Ni_{11}Se_2(CO)_{18}]^{2-}$,[75] as well as P incorporation into Ni NPs.[85] These results also help explain why no thiolate-stabilized Ni APNCs have been isolated thus far, despite their ubiquity for group 11.[2, 19-21] Because Ni(0) is so reducing (Table x-1), C-S oxidative addition at low-valent Ni is facile, which results in net oxidation of the Ni atom and destruction of the thiolate ligand.

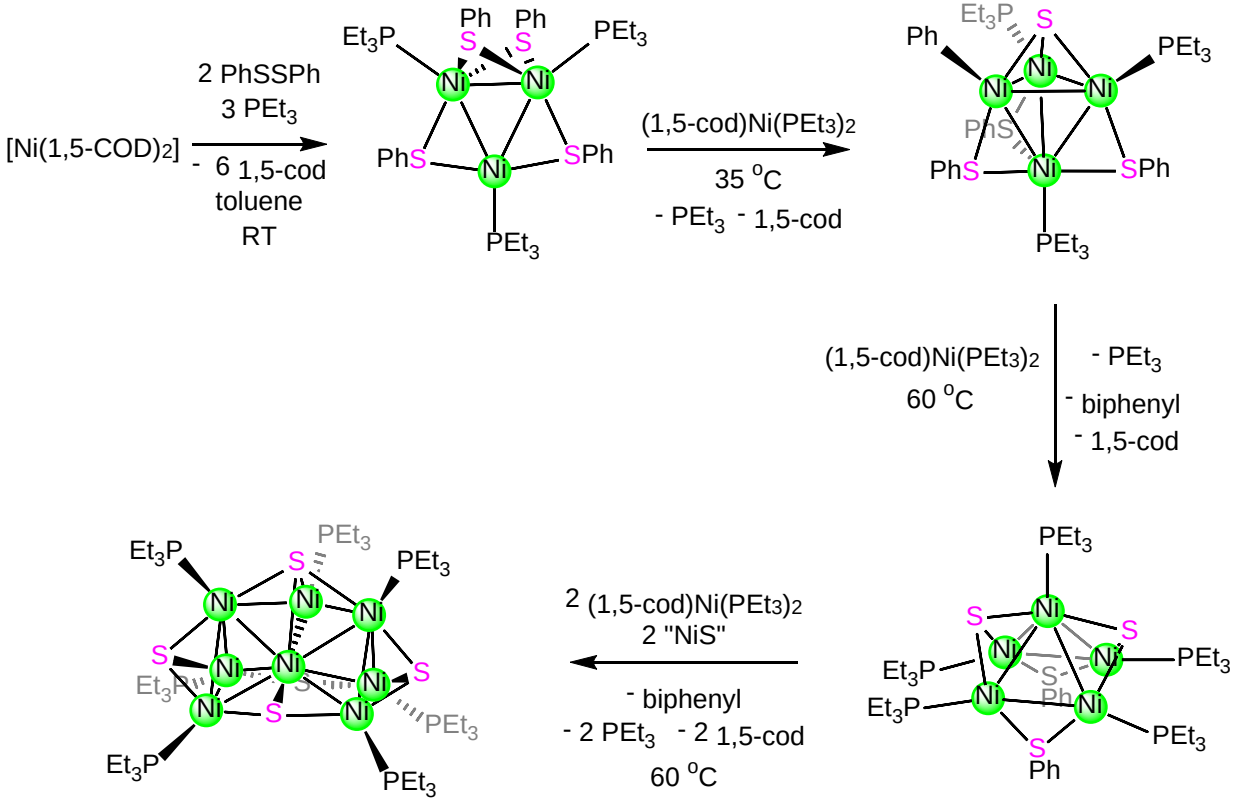

Scheme x-3. Synthesis of $[Ni_8(S)_5(PEt_3)_7]$ from $[Ni(1,5\text{-}COD)_2]$

x.4 Synthesis of Co APNCs

As was seen for group 10, the earliest attempts to make large cobalt clusters focused on the use of carbon monoxide as the supporting ligand. For example, Chini reported the synthesis of $[Co_6(CO)_{15}]^{2-}$ in 1967,[32, 88-89] and despite its synthesis over five decades ago, it remains the largest reported homoleptic cobalt carbonyl cluster known. It was synthesized by reduction of $[Co_4(CO)_{12}]$ with lithium or sodium metal in THF,[88] a route that has also been employed to make Ni and Fe carbonyl clusters.[32] As was observed for

Ni, larger cobalt carbonyl clusters typically feature interstitial main group atoms, most commonly carbon. As a result, these larger clusters do not fit our definition of an APNC. That said, there is at least one Co-containing cluster type that meets our strict definition of an APNC, namely, $[Co_9Te_6(CO)_8]^{n-}$ (n = 1, 2).[90-93] These clusters were prepared by reaction of $[Cp'_2Nb(\eta^2\text{-}Te_2)H]$ (Cp' = $^tBuC_5H_4$) with MeLi, followed by addition of $[Co_2(CO)_8]$, followed by cation exchange with [PPN][Cl]. Mechanistic studies suggest that the first step of the reaction results in formation of a mixture of $[Cp'_2Nb(Te)Me]$, $[Cp'_2Nb(H)_2(TeMe)]$, and $[Cp'_2Nb(TeMe)_2]$.[94] These species function as good Te-atom transfer reagents, presumably because of the mismatch between the hard acid (Nb) and soft base (Te) results in weak Nb-Te bonds. Additionally, the Cp'_2Nb fragment function as a CO trap during the reaction, forming the Nb(III) cation, $[Cp'_2Nb(CO)_2]^+$. Its formation apparently allows Co cluster growth by decreasing the pool of available CO in the reaction mixture. The mixture of telluride-supported niobium metallocenes oxidize $[Co_2(CO)_8]$ to form a mixture of $[Co_9Te_6(CO)_8]^{n-}$ (n = 1, 2), which are then converted into the $[PPN]^+$ salts by cation exchange. The two clusters could be separated by selective crystallization and could be isolated in 28% total yield. In the solid state, both the -1 and -2 clusters feature a $[Co_9]$ cobalt-centered cubic kernel (Figure x-9). The metrical parameters of the two derivatives are nearly identical. The average Co_{center}-Co_{shell} distance is 2.40 Å, which is considerable shorter that the Co-Co distance in the bulk metal (2.49 Å),[95] whereas the average Co_{center}-Te distance is 2.98 Å, demonstrating that there is little interaction between these atoms. Thus, the interstitial cobalt is only bound to the eight outer cobalt atoms and no other atoms. Calculations suggest that the frontier orbitals are closely-spaced and delocalized over the $[Co_9Te_6(CO)_8]^{n-}$ cage.[93] The -1 cluster is predicted to have a $(e_g)^2(t_{1g})^0$ open shell ground state. However, magnetism measurements reveal a room temperature moment of 4.65 μ_B, which is the value expected for an S = 2 state. The authors suggest that mixing of a low-lying excited state with the ground state may account for the observed magnetic properties. The neutral cluster $[Co_9Te_6(CO)_4(PPh_3)_4]$ is also known, but has not been well studied.[93] Nonetheless, calculations suggests that its lone unpaired electron resides principally upon the interstitial cobalt atom. The use of a Co(0)-containing precursor in this reaction, i.e., $[Co_2(CO)_8]$, is likely key to its success, as attempts to make low-valent Co APNCs using Co^{2+} salts can fail to achieve metal reduction.[96]

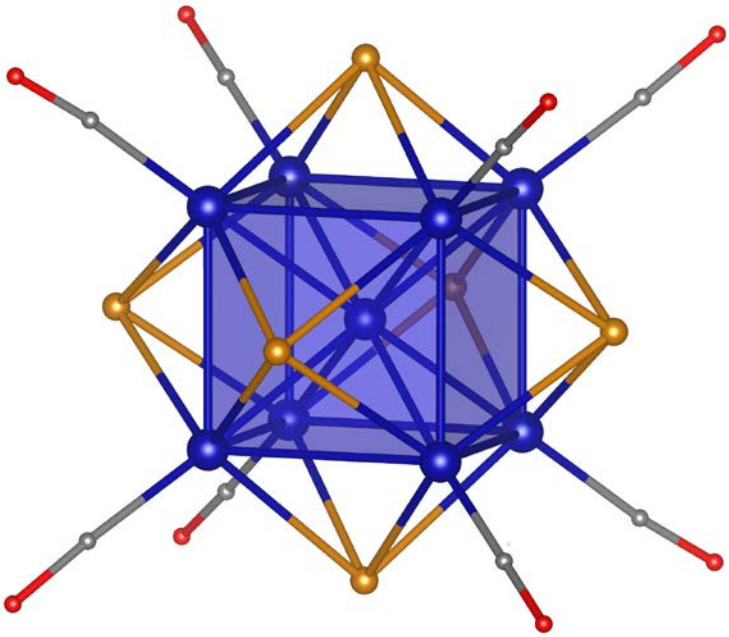

Figure x-9. Solid-state structure of [PPN][$Co_9Te_6(CO)_8$]. Co, Te, C, and O atoms are shown in blue, goldenrod, grey, and red, respectively. The blue polyhedron represents the coordination sphere of the central Co atom. [PPN]$^+$ counterion omitted for clarity. Data taken from Ref. [93].

The reaction of [$Cp^*_2Nb(\eta^2\text{-}Te_2H)$] with [$Co_2(CO)_8$] in refluxing toluene also produces [$Co_9Te_6(CO)_8$]$^{n-}$ (n = 1, 2), in addition to the larger clusters, [$Cp^*_2Nb(CO)_2$][$Co_{11}Te_5(CO)_{15}$] and [$Cp^*_2Nb(CO)_2$][$Co_{11}Te_7(CO)_{10}$].[97] While neither of these latter clusters qualifies as an APNC, their formation demonstrates the complex energy landscape that is present during the reaction, and highlights how hard it is to control speciation during the synthesis of APNCs. An analysis of their structures and bonding is also informative. In this solid state, [$Cp^*_2Nb(CO)_2$][$Co_{11}Te_5(CO)_{15}$] features a [$Co_{11}Te_2$] cobalt-centered bi-capped pentagonal prism kernel. The two Te^{2-} ligands occupy the capping sites and feature μ_5 binding modes. In addition, three of the five square faces of the pentagonal prism are bridged by μ_4-Te ligands, while the remaining two square faces are bridged by CO ligands. Each outer Co center also features one terminal CO ligand. [$Cp^*_2Nb(CO)_2$][$Co_{11}Te_7(CO)_{10}$] also features a [$Co_{11}Te_2$] cobalt-centered bi-capped pentagonal prism kernel.[90, 98] As seen with [$Co_{11}Te_5(CO)_{15}$]$^-$, the two Te^{2-} ligands occupy the capping sites and feature μ_5 binding modes. However, each square face of the pentagonal prism is bridged by μ_4-Te ligands. Each outer Co center also features one terminal CO ligand. The closely related cluster, [PPh_4]$_2$[$Co_{11}Te_7(CO)_{10}$], can be prepared by reaction of [$Co_2(CO)_8$] with Na_2Te_2 and [Ph_4P]Cl in methanol

under solvothermal conditions.[99] The authors propose that the oxidation state of central Co is 2+, whereas the outer Co atoms are in the 1+ oxidation state. In addition, several Co-containing clusters built around $[Co_9Bi_4]$ anti-cuboctahedral kernels are known, including $[Bi_4Co_9(CO)_{16}]^{2-}$ and $[Bi_8Co_{14}(CO)_{20}]$.[100] These clusters were formed by oxidation of a $[PPN][Bi_2Co_4(CO)_{11}]/[Mo(CO)_3(\eta^6\text{-toluene})]$ mixture with air. While the reaction did not generate an APNC, owing to the inclusion of Bi into the anti-cuboctahedral kernel, it provides another example of the use of a CO trap (in this case $[Mo(CO)_3(\eta^6\text{-toluene})]$) to increase cluster nuclearity.

The challenges inherent in Co APNC synthesis are also exemplified by the reactivity of $CoCl_2$ with $PhCH_2CH_2SH$ under modified Brust/Schiffrin conditions.[96] In particular, reaction of $CoCl_2$ with excess $PhCH_2CH_2SH$ and $NaBH_4$ in THF at room temperature resulted in formation of the $[Co_{10}(SR)_{16}Cl_4]$ in 37% yield (Scheme x-4). In the solid state, this cluster features a T3 supertetrahedral structure with 12 doubly-bridged thiolate ligands and four triply-bridged thiolate ligands. The four Cl^- ligands occupy the corners of the supertetrahedron. Importantly, every Co center in this cluster is Co(II), demonstrating that, despite the use of Brust/Schiffrin conditions, no metal reduction is occurring. This observation can be rationalized by the relatively high $2e^-$ reduction potential of Co^{2+} (Table x-1).

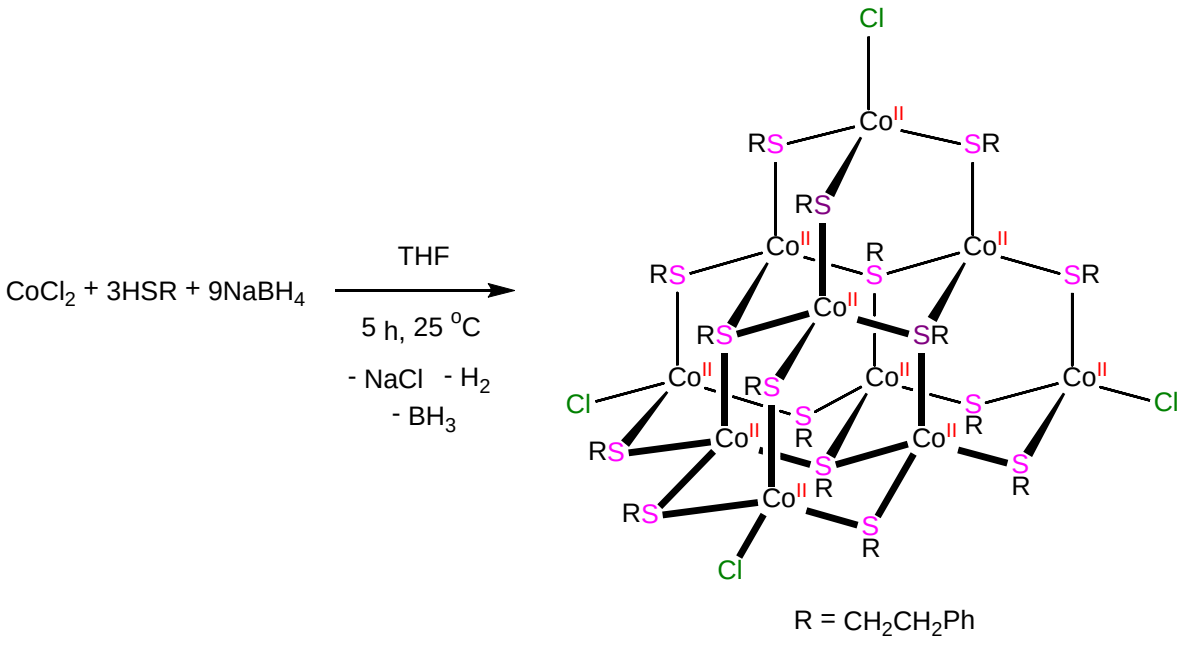

Scheme x-4. Synthesis of $[Co_{10}(SR)_{16}Cl_4]$ using modified Brust/Schiffrin conditions

x.5 Attempted Synthesis of Fe APNCs

Thus far, no Fe APNCs are known, according to the definition of APNCs adopted for this chapter, despite the long and rich history of iron cluster chemistry.[31, 101-102] As with Section x-3 and Section x-4, we will start the discussion with metal carbonyl clusters. In this regard, several iron carbonyl clusters have been synthesized via the oligomerization of $[Fe(CO)_5]$; however, the highest nuclearity homoleptic iron carbonyl cluster made via this route is $[Fe_4(CO)_{13}]^{2-}$.[32] Larger iron carbonyl clusters have been isolated, but they feature other co-ligands as well, most notably carbide (C^{4-}), as observed in the case of $[Fe_5(\mu_5\text{-}C)(CO)_{15}]$ and $[Fe_6(\mu_6\text{-}C)(CO)_{16}]^{2-}$.[32, 103-105] Intriguingly, the interstitial carbide ligand in these examples is formed via disproportionation of carbon monoxide (eq 1, Scheme x-5),[32] which forms CO_2 as a by-product. For example, reduction of $[Fe(CO)_5]$ with $[Mn(CO)_5]^-$ in refluxing diglyme results in formation of $[Fe_6(\mu_6\text{-}C)(CO)_{16}]^{2-}$ and CO_2, in low yields (eq 2, Scheme x-5).[104-105] This transformation, which proceeds via an $[MnFe_2(CO)_{12}]^-$ intermediate, is likely promoted by the highly reducing nature of Fe(0), and can be rationalized by the Fe:CO ratio, which increases as the cluster nuclearity increases. This increase is significant because fewer CO ligands per Fe atoms means that each Fe atom is more electron rich and therefore more likely to reduce CO. As a result of the CO disproportionation, the resulting carbide cluster features an average Fe oxidation state that is higher than the zero oxidation state expected for a homoleptic Fe carbonyl cluster. In particular, the average Fe oxidation state of $[Fe_6(\mu_6\text{-}C)(CO)_{16}]^{2-}$ is +0.33. Similar CO disproportionation chemistry has been reported for Ru.[106]

$$2\ CO + 4\ e^- \longrightarrow C^{4-} + CO_2 \qquad (1)$$

$$[Fe(CO)_5] + [Mn(CO)_5]^- \xrightarrow[\text{reflux, 1 h}]{\text{diglyme}} [Fe_6C(CO)_{16}]^{2-} + CO_2 + CO \qquad (2)$$

Scheme x-5. CO disproportionation reactions

The observation of spontaneous CO disproportionation during the oligomerization of $[Fe(CO)_5]$ implies that the Fe(0) core in a putative Fe APNC will be highly reducing. Accordingly, it is clear that the passivating ligands must resistant to reduction. However, many commonly-used ligands in APNC synthesis, such as thiolates and phosphines are not resistant to reduction, as was shown in Section x-3. Not surprisingly, several reports of Fe NP (and amorphous Fe) syntheses using $[Fe(CO)_5]$ as a precursor do mention carbon

contamination in the isolated material.[107-110] It seems likely that carbon incorporation into these materials occurs via the CO disproportionation reaction described in Scheme x-5.

Many chalcogenide- and thiolate-supported Fe clusters are known,[102, 111] but none obey our definition of an APNC. These clusters are typically made by reacting $FeCl_2$ with $E(SiMe_3)$ (E = S, Se),[112-113] often in the presence of a phosphine. For example, reaction of $FeCl_2$, PEt_3, and $S(SiMe_3)_2$ in THF results in formation of $[Fe_7S_6(PEt_3)_4Cl_3]$, which converts to $[Fe_6S_6(PEt_3)_4Cl_2]$ on standing (Eq 1 and 2, Scheme x-6).[114-116] They feature average Fe oxidation states of +2.14 and +2.33, respectively. To account for the +2.14 oxidation state in $[Fe_7S_6(PEt_3)_4Cl_3]$, and the increase in oxidation state on converting to $[Fe_6S_6(PEt_3)_4Cl_2]$, it is likely that some Fe^{2+} ions are undergoing disproportionation during the reaction, forming unidentified Fe(0) or Fe(I) by-products. In fact, Holm and co-workers note the formation of dark insoluble material during the conversion of $[Fe_7S_6(PEt_3)_4Cl_3]$ to $[Fe_6S_6(PEt_3)_4Cl_2]$,[116] which could correspond to these reduced products. For comparison, reaction of $[NiCl_2(PEt_2Ph)_2]$ with $Se(SiMe_3)_2$ result is successful generation of the Ni APNC, $[Ni_{21}Se_{14}(PEt_2Ph)_{12}]$ (Section x-3),[56] which features an average Ni oxidation state of +1.33. In this example, the average oxidation state of Ni actually decreases over the course of the reaction. Another relevant Fe cluster, $[NBu_4]_2[Fe_4S_4Br_4]$, was prepared by reaction of $FeBr_3$ with Na_2S and $[NBu_4][Br]$ in DMF.[117] In this case, Na_2S is the reducing agent and S_8 is formed as a by-product. Its average Fe oxidation state is +2.5. The chloride and iodide congeners are also known.[118] Similarly, reaction of $[Fe(H_2O)_6][BF_4]_2$ with PEt_3 and H_2Se in the presence of $[NBu_4][PF_6]$ in EtOH/acetone results in formation of $[Fe_6(\mu_3{-}Se)_8(PEt_3)_6][PF_6]$.[119] The average Fe oxidation state for this cluster is +2.83.

$$FeCl_2 + PEt_3 + S(SiMe_3)_2 \xrightarrow[RT,\ 24\ h]{THF} [Fe_7S_6(PEt_3)_4Cl_3] \qquad (1)$$

$$[Fe_6S_6(PEt_3)_4Cl_2] \xleftarrow[22\ h]{CHCl_3} \qquad (2)$$

$$Fe + S_8 + I_2 + [NEt_4][I] \xrightarrow[Reflux,\ 24\ h]{THF} [NEt_4]_2[Fe_6S_6I_6] \qquad (3)$$

Scheme x-6. Synthesis of Fe chalcogenide clusters.

Several Fe chalcogenide clusters have been prepared from Fe(0) starting materials, as well, but they typically display Fe oxidation states ≥ 2, in contrast to Co and Ni clusters made by similar routes. For example, $[NEt_4]_2[Fe_6S_6I_6]$ was prepared by reaction of Fe metal with S_8, I_2, and $[NEt_4][I]$ (Eq 3, Scheme x-6),[120] while $[NBu_4]_2[Fe_6E_6(NO)_6]$ (E = S, Se), was prepared by the solvothermal reactions of $[NBu_4][Fe(CO)_3NO]$ with Se or S_8 in methanol.[121] $[Fe_6S_6I_6]^{2-}$ features an average Fe oxidation state of +2.67. Also of note, reaction of the Fe(0) synthon $[(IEt_2Me_2)_2Fe(dvtms)]$ (IEt_2Me_2 = 1,3-diethyl-4,5-dimethylimidazol-2-ylidene; dvtms = divinyltetramethyldisiloxane) with 1 equiv of Se or 0.125 equiv of S_8 results in the formation of $[(IEt_2Me_2)_4Fe_4E_4]$ (E = S, Se), which represents an unusually reduced iron chalcogenide cluster.[113, 122] Its average Fe oxidation state of +2. Cyclic voltammetry of the closely related cluster, $[NBu_4]_4[Fe_4S_4(CN)_4]$, confirms that the $[Fe_4E_4]^0$ core is highly reducing.[123] In particular, this cluster features a reversible $1e^-$ oxidation potential of -1.42 V in MeCN (vs. SCE), despite the presence of the electron withdrawing cyanide ligands. It is not surprising then that more highly reduced iron chalcogenide clusters have eluded isolation.

x.6 Conclusions and Outlook

As is hopefully apparent from the Sections above, there are a number of inter-related reasons why APNCs of Fe, Co, and Ni are so exceptionally rare. Some of these reasons are inherent to their material properties and some are practical. One practical reason why these materials are so rare is due to their enhanced air sensitivity, especially relative to the group 11 APNCs.[30] This aspect of their chemistry is nicely illustrated by $[Ni_{23}Se_{12}Cl_3(PEt_3)_{10}]$, which is not only air-sensitive, but also rapidly react with CH_2Cl_2.[57] Both observations demonstrate the care required to work with this cluster. $[Co_9Te_6(CO)_4(PPh_3)_4]$ is also highly air sensitive,[93] as is $[Co_{10}(SR)_{16}Cl_4]$,[96] and many of the Fe chalcogenide clusters described in Section x-5.[102, 111] While daunting, this challenge can actually be overcome by the implementation of air-free synthetic procedures and rigorous purification of starting materials and solvents. In his regard, it would be helpful to adopt the experimental protocols of organometallic chemists, who have been synthesizing and characterizing highly air-sensitive metal complexes for decades. These procedures and protocols have been described in detail.[124-125]

The high reduction potentials often displayed by these cluster also restricts the choice of available co-ligands. This fact is nicely illustrated by the attempted preparation of phenylthiolate-protected Ni APNCs from [Ni(1,5-COD)$_2$] and PhSSPh.[76] In this example, the phenylthiolate is reduced to biphenyl and sulfide, providing [Ni$_8$(S)$_5$(PEt$_3$)$_7$] among other products. Similar reduction chemistry is observed during the reaction of Ni(η^3-CPh$_3$)$_2$ with PPh$_3$,[84] which results in formation of biphenyl, along with [Ni$_3$(μ_3-PPh)(μ-PPh$_2$)$_2$(PPh$_3$)$_3$]. The synthesis of [Ni$_8$(CN^{t}Bu)$_{12}$][Cl] illustrates a similar effect.[87] In this example, the ligand does not undergo fragmentation upon reduction. Instead, it undergoes a change in binding mode – from η^1 to μ-η^2:η^1 – which promotes the formation of the nanosheet structure and disfavors the formation of the highly compact metal core required to form an APNC. Given these examples, it is not surprising then that all authentic Co- and Ni-containing APNCs isolated thus far are stabilized by dianionic chalcogenide ligands, i.e., E^{2-}, which are unable to undergo further reduction chemistry. Consequently, it is clear that future work should focus on the use of reduction-resistant ligands to stabilize APNCs of Fe, Co, and Ni, such as Cl^-, Br^-, I^-, S^{2-}, Te^{2-}, and P^{3-}. These ligands could be used in combination with neutral Lewis bases that are also reduction-resistant, such as PEt$_3$, which appears to be well-suited for this purpose, although there are certainly other reduction-resistant Lewis bases that could also be employed. That said, it is obvious that this list is somewhat restrictive. Halide, chalogenide, and pnictinide ligands do not possess R groups, which eliminates an important tool that synthetic chemists have for modifying structure and function. This modifiability has been used to great effect in thiolate-protected group 11 APNC chemistry. However, until thiolate ligands can be designed that do not undergo C-S oxidative addition, this popular ligand class will likely not be useful for stabilizing APNCs of Fe, Co, and Ni. The design and synthesis of reduction-resistant thiolate ligands will likely be an important research direction in the coming years.

Uncontrolled redox chemistry has also played an important role in the speciation of chalcogenide-supported Fe clusters, as exemplified by [Fe$_7$S$_6$(PEt$_3$)$_4$Cl$_3$], [Fe$_6$S$_6$(PEt$_3$)$_4$Cl$_2$], and related clusters.[114-116] In these examples, unwanted disproportionation of a lower-valent intermediate cluster leads to the isolation of the high oxidation state products. Thus, access to an Fe(0)-containing APNC will require suppression of this unwanted disproportionation. Alternatively, it could potentially be harnessed to access low-valent materials, provided the desired low-valent product can be separated from the reaction by-products. However, it is not

readily apparent how these disproportionation reactions can be controlled, making this task much easier said than done.

Looking to the future, there are several avenues of investigation that promise to expand our knowledge of APNC synthesis, structure, and bonding. For example, it is clear that APNCs of Fe, Co, and Ni usually feature open shell electronic structures, which contrasts with the closed shell configurations typically observed for group 11 APNCs.[2, 19-21] Open shell APNCs with large spin states and a high degree of metal-metal bonding, which leads to manifold of closely-spaced electronic states near the HOMO-LUMO gap, could feature interesting magnetic properties, such as single molecule magnetism and metamagnetism. These properties could eventually be harnessed for a variety of potential applications, including magnetic data storage and quantum computing.[3, 10-12] Another area of interest is the synthesis of heterometallic APNCs of Fe, Co, and Ni.[126] Previously work on nanoparticles has shown that alloying can greatly modify their magnetic properties. For example, face-centered tetragonal FePt NPs exhibit higher coercivities than comparably sized Fe NPs,[127-128] due to the magnetic coupling of the Fe and Pt *n*d states.[126] Heterometallic FeCo APNCs are also an intriguing target, given the high magnetic moment that is expected for this combination.[129] However, the challenges inherent in the synthesis of homometallic APNCs, as discussed above, are even more acute for the synthesis of heterometallic APNCs. Their successful synthesis will require the discovery of an appropriate combination of capping ligands and metal atom precursors, coupled with the need to reproducibly incorporate an exact number of each metal atom into the APNC. This challenging synthetic problem will likely remain unsolved for some time.

Acknowledgement

I thank the National Science Foundation (CHE 1764345) for financial support of this work. I also thank Alexander J. Touchton for assistance with the preparation of the VESTA image files.

References

[1] M. Walter, J. Akola, O. Lopez-Acevedo, P. D. Jadzinsky, G. Calero, C. J. Ackerson, R. L. Whetten, H. Grönbeck, H. Häkkinen, A unified view of ligand-protected gold clusters as superatom complexes. *Proc. Natl. Acad. Sci.*, 2008, **105**, 9157-9162.

[2] I. Chakraborty, T. Pradeep, Atomically Precise Clusters of Noble Metals: Emerging Link between Atoms and Nanoparticles. *Chem. Rev.*, 2017, **117**, 8208-8271.

[3] C. Busche, L. Vilà-Nadal, J. Yan, H. N. Miras, D.-L. Long, V. P. Georgiev, A. Asenov, R. H. Pedersen, N. Gadegaard, M. M. Mirza, D. J. Paul, J. M. Poblet, L. Cronin, Design and fabrication of memory devices based on nanoscale polyoxometalate clusters. *Nature*, 2014, **515**, 545.

[4] G. Li, R. Jin, Atomically Precise Gold Nanoclusters as New Model Catalysts. *Acc. Chem. Res.*, 2013, **46**, 1749-1758.

[5] L. Liu, A. Corma, Metal Catalysts for Heterogeneous Catalysis: From Single Atoms to Nanoclusters and Nanoparticles. *Chem. Rev.*, 2018, **118**, 4981-5079.

[6] A. W. Cook, Z. R. Jones, G. Wu, S. L. Scott, T. W. Hayton, An Organometallic Cu_{20} Nanocluster: Synthesis, Characterization, Immobilization on Silica, and "Click" Chemistry. *J. Am. Chem. Soc.*, 2018, **140**, 394-400.

[7] L.-Y. Chen, C.-W. Wang, Z. Yuan, H.-T. Chang, Fluorescent Gold Nanoclusters: Recent Advances in Sensing and Imaging. *Anal. Chem.*, 2015, **87**, 216-229.

[8] M. Colombo, S. Carregal-Romero, M. F. Casula, L. Gutierrez, M. P. Morales, I. B. Bohm, J. T. Heverhagen, D. Prosperi, W. J. Parak, Biological applications of magnetic nanoparticles. *Chem. Soc. Rev.*, 2012, **41**, 4306-4334.

[9] L. Lisnard, F. Tuna, A. Candini, M. Affronte, R. E. P. Winpenny, E. J. L. McInnes, Supertetrahedral and Bi-supertetrahedral Cages: Synthesis, Structures, and Magnetic Properties of Deca- and Enneadecametallic Cobalt(II) Clusters. *Angew. Chem. Int. Ed.*, 2008, **47**, 9695-9699.

[10] D.-L. Long, R. Tsunashima, L. Cronin, Polyoxometalates: Building Blocks for Functional Nanoscale Systems. *Angew. Chem. Int. Ed.*, 2010, **49**, 1736-1758.

[11] A. Gaita-Ariño, F. Luis, S. Hill, E. Coronado, Molecular spins for quantum computation. *Nat. Chem.*, 2019, **11**, 301-309.

[12] J. Tejada, E. M. Chudnovsky, E. del Barco, J. M. Hernandez, T. P. Spiller, Magnetic qubits as hardware for quantum computers. *Nanotechnology*, 2001, **12**, 181.

[13] R. Jin, Quantum sized, thiolate-protected gold nanoclusters. *Nanoscale*, 2010, **2**, 343-362.

[14] X. Kang, H. Chong, M. Zhu, $Au_{25}(SR)_{18}$: the captain of the great nanocluster ship. *Nanoscale*, 2018, **10**, 10758-10834.

[15] M. W. Heaven, A. Dass, P. S. White, K. M. Holt, R. W. Murray, Crystal Structure of the Gold Nanoparticle $[N(C_8H_{17})_4][Au_{25}(SCH_2CH_2Ph)_{18}]$. *J. Am. Chem. Soc.*, 2008, **130**, 3754-3755.

[16] The [M13] kernel can also adopt cuboctahedral and anti-cuboctahedral arrangements.:

[17] J. G. Brennan, T. Siegrist, S. M. Stuczynski, M. L. Steigerwald, The transition from molecules to solids: molecular syntheses of $Ni_9Te_6(PEt_3)_8$, $Ni_{20}Te_{18}(PEt_3)_{12}$ and NiTe. *J. Am. Chem. Soc.*, 1989, **111**, 9240-9241.

[18] N. Keiko, O. Satoru, Y. Tadashi, I. Tasuku, W. Seiji, N. Masami, Synthesis and Characterization of the Au_{11} Cluster with Sterically Demanding Phosphine Ligands by Single Crystal X-ray Diffraction and XPS Spectroscopy. *Bull. Chem. Soc. Jpn*, 2003, **76**, 1601-1602.

[19] R. Jin, C. Zeng, M. Zhou, Y. Chen, Atomically Precise Colloidal Metal Nanoclusters and Nanoparticles: Fundamentals and Opportunities. *Chem. Rev.*, 2016, **116**, 10346-10413.

[20] X. Du, R. Jin, Atomic-precision engineering of metal nanoclusters. *Dalton Trans.*, 2020, **49**, 10701-10707.

[21] X. Kang, Y. Li, M. Zhu, R. Jin, Atomically precise alloy nanoclusters: syntheses, structures, and properties. *Chem. Soc. Rev.*, 2020, **49**, 6443-6514.

[22] A. Zabala-Lekuona, J. M. Seco, E. Colacio, Single-Molecule Magnets: From Mn_{12}-ac to dysprosium metallocenes, a travel in time. *Coord. Chem. Rev.*, 2021, **441**, 213984.

[23] R. Hernández Sánchez, T. A. Betley, Meta-Atom Behavior in Clusters Revealing Large Spin Ground States. *J. Am. Chem. Soc.*, 2015, **137**, 13949-13956.

[24] K. Chakarawet, P. C. Bunting, J. R. Long, Large Anisotropy Barrier in a Tetranuclear Single-Molecule Magnet Featuring Low-Coordinate Cobalt Centers. *J. Am. Chem. Soc.*, 2018, **140**, 2058-2061.

[25] K. Chakarawet, M. Atanasov, J. Marbey, P. C. Bunting, F. Neese, S. Hill, J. R. Long, Strong Electronic and Magnetic Coupling in M_4 (M = Ni, Cu) Clusters via Direct Orbital Interactions between Low-Coordinate Metal Centers. *J. Am. Chem. Soc.*, 2020, **142**, 19161-19169.

[26] J. M. Frost, K. L. M. Harriman, M. Murugesu, The rise of 3-d single-ion magnets in molecular magnetism: towards materials from molecules? *Chem. Sci.*, 2016, **7**, 2470-2491.

[27] A. W. Cook, T. W. Hayton, Case Studies in Nanocluster Synthesis and Characterization: Challenges and Opportunities. *Acc. Chem. Res.*, 2018, **51**, 2456-2464.

[28] A. W. Cook, Z. R. Jones, G. Wu, S. J. Teat, S. L. Scott, T. W. Hayton, Synthesis and Characterization of "Atlas-Sphere" Copper Nanoclusters: New Insights into the Reaction of Cu^{2+} with Thiols. *Inorg. Chem.*, 2019, **58**, 8739-8749.

[29] Y. R. Luo, *Comprehensive Handbook of Chemical Bond Energies*, CRC Press, Boca Raton, FL, 2007.

[30] S. G. Bratsch, Standard Electrode Potentials and Temperature Coefficients in Water at 298.15 K. *J. Phys. Chem. Ref. Data*, 1989, **18**, 1-21.

[31] E. L. Muetterties, T. N. Rhodin, E. Band, C. F. Brucker, W. R. Pretzer, Clusters and surfaces. *Chem. Rev.*, 1979, **79**, 91-137.

[32] C. Cesari, J.-H. Shon, S. Zacchini, L. A. Berben, Metal carbonyl clusters of groups 8–10: synthesis and catalysis. *Chem. Soc. Rev.*, 2021, **50**, 9503-9539.

[33] E. G. Mednikov, L. F. Dahl, Syntheses, structures and properties of primarily nanosized homo/heterometallic palladium CO/PR_3-ligated clusters. *Philos. Trans. R. Soc. A*, 2010, **368**, 1301-1332.

[34] I. Ciabatti, C. Femoni, M. C. Iapalucci, G. Longoni, S. Zacchini, Platinum Carbonyl Clusters Chemistry: Four Decades of Challenging Nanoscience. *J. Cluster Sci.*, 2014, **25**, 115-146.

[35] J. K. Beattie, A. F. Masters, J. T. Meyer, Nickel carbonyl cluster complexes. *Polyhedron*, 1995, **14**, 829-868.

[36] A. F. Masters, J. T. Meyer, Polyhedron report number 51 Structural systematics in nickel carbonyl cluster anions. *Polyhedron*, 1995, **14**, 339-365.

[37] T. A. Stromnova, I. I. Moiseev, Palladium carbonyl complexes. *Russ. Chem. Rev.*, 1998, **67**, 485-514.

[38] C. Femoni, M. C. Iapalucci, F. Kaswalder, G. Longoni, S. Zacchini, The possible role of metal carbonyl clusters in nanoscience and nanotechnologies. *Coord. Chem. Rev.*, 2006, **250**, 1580-1604.

[39] B. Berti, C. Femoni, M. C. Iapalucci, S. Ruggieri, S. Zacchini, Functionalization, Modification, and Transformation of Platinum Chini Clusters. *Eur. J. Inorg. Chem.*, 2018, **2018**, 3285-3296.

[40] A. Ceriotti, P. Chini, R. Della Pergola, G. Longoni, Carbonylnickelates. 3. Synthesis and chemical characterization of the $[Ni_{12}(CO)_{21}H_{4-n}]^{n-}$ (n = 2, 3, 4) clusters. *Inorg. Chem.*, 1983, **22**, 1595-1598.

[41] R. W. Broach, L. F. Dahl, G. Longoni, P. Chini, A. J. Schultz, J. M. Williams, in *Transition Metal Hydrides, Vol. 167*, American Chemical Society, **1978**, pp. 93-110.

[42] J. V. Barkley, T. Eguchi, R. A. Harding, B. T. Heaton, G. Longoni, L. Manzi, H. Nakayama, K. Miyagi, A. K. Smith, A. Steiner, Solid state studies (X-ray and ^{1}H-, ^{13}C-NMR) on $(NMe_4)_{4-x}[H_xNi_{12}(CO)_{21}]\cdot S$ (x=1, S=Me_2CO; x=2, S=2THF). *J. Organomet. Chem.*, 1999, **573**, 254-260.

[43] A. Ceriotti, A. Fait, G. Longoni, G. Piro, F. Demartin, M. Manassero, N. Masciocchi, M. Sansoni, Synthesis and x-ray structure of the $[HNi_{38}(CO)_{42}C_6]^{5-}$ cluster: an extended fragment of the $Cr_{23}C_6$ lattice stabilized in a molecular carbonyl nickel cluster. *J. Am. Chem. Soc.*, 1986, **108**, 8091-8092.

[44] F. Calderoni, F. Demartin, M. C. Iapalucci, G. Longoni, Synthesis and Crystal Structure of the $[Ni_{32}C_6(CO)_{36}]^{6-}$ Hexaanion: An Extended Fragment of the $M_{23}C_6$ Lattice Stabilized in a Shell of Edge-Bridging Carbonyl Ligands. *Angew. Chem. Int. Ed.*, 1996, **35**, 2225-2226.

[45] A. Ceriott, F. Demartin, G. Longoni, M. Manassero, M. Marchionna, G. Piva, M. Sansoni, Synthesis and Structure of the $[Ni_{38}Pt_6(CO)_{48}H_{6-n}]^{n-}$ (n=5, 4) Ions: Ni-Pt Clusters as Models for "Cherry" Crystallites. *Angew. Chem. Int. Ed.*, 1985, **24**, 697-698.

[46] F. Fabrizi de Biani, C. Femoni, M. C. Iapalucci, G. Longoni, P. Zanello, A. Ceriotti, Redox Behavior of $[H_{6-n}Ni_{38}Pt_6(CO)_{48}]^{n-}$ (n = 4−6) Anions: A Series of Metal Carbonyl Clusters Displaying Electron-Sink Features. *Inorg. Chem.*, 1999, **38**, 3721-3724.

[47] N. de Silva, L. F. Dahl, Aprotic Synthesis and Structural Determination of the Nanosized Nonprotonated ν_3-Octahedral $[Pt_6Ni_{38}(CO)_{48}]^{6-}$ Hexaanion Stabilized as a Cubic Solvated $[NMe_4]^+$ Salt. *Inorg. Chem.*, 2006, **45**, 8814-8816.

[48] C. Femoni, M. C. Iapalucci, G. Longoni, P. H. Svensson, P. Zanello, F. Fabrizi de Biani, Synthesis and Characterisation of ν_3-Octahedral $[Ni_{36}Pd_8(CO)_{48}]^{6-}$ and $[Ni_{35}Pt_9(CO)_{48}]^{6-}$ Clusters Displaying Unexpected Surface Segregation of Pt Atoms and Molecular and/or Crystal Substitutional Ni/Pd and Ni/Pt Disorder. *Chem. Eur. J.*, 2004, **10**, 2318-2326.

[49] N. T. Tran, M. Kawano, D. R. Powell, L. F. Dahl, High-nuclearity $[Pd_{13}Ni_{13}(CO)_{34}]^{4-}$ containing a 26-atom $Pd_{13}Ni_{13}$ core with an unprecedented five-layer close-packed triangular stacking geometry: possible substitutional Pd/Ni crystal disorder at specific intralayer nickel sites *J. Chem. Soc., Dalton Trans.*, 2000, 4138-4144.

[50] C. Femoni, M. C. Iapalucci, G. Longoni, P. H. Svensson, J. Wolowska, Homoleptic Carbonyl Ni–Pd Clusters: Synthesis of $[Ni_{16}Pd_{16}(CO)_{40}]^{4-}$ and $[Ni_{26}Pd_{20}(CO)_{54}]^{6-}$ and Structural Characterization of $[N^nBu_4]_4[Ni_{16}Pd_{16}(CO)_{40}]$. *Angew. Chem. Int. Ed.*, 2000, **39**, 1635-1637.

[51] M. Kawano, J. W. Bacon, C. F. Campana, B. E. Winger, J. D. Dudek, S. A. Sirchio, S. L. Scruggs, U. Geiser, L. F. Dahl, High-Nuclearity Close-Packed Palladium-Nickel Carbonyl Phosphine Clusters: Heteropalladium $[Pd_{16}Ni_4(CO)_{22}(PPh_3)_4]^{2-}$ and $[Pd_{33}Ni_9(CO)_{41}(PPh_3)_6]^{4-}$ Containing Pseudo-T_d ccp $Pd_{16}Ni_4$ and Pseudo-D_{3h} hcp $Pd_{33}Ni_9$ Cores. *Inorg. Chem.*, 2001, **40**, 2554-2569.

[52] N. T. Tran, M. Kawano, D. R. Powell, R. K. Hayashi, C. F. Campana, L. F. Dahl, Isostructural $[Au_6Pd_6(Pd_{6-x}Ni_x)Ni_{20}(CO)_{44}]^{6-}$ and $[Au_6Ni_{32}(CO)_{44}]^{6-}$ Clusters Containing Corresponding Nonstoichiometric $Au_6Pd_6(Pd_{6-x}Ni_x)Ni_{20}$ and Stoichiometric Au_6Ni_{32} Nanosized Cores: Substitutional

Pd/Ni Crystal Disorder (Coloring Problem) at Only Six Specific Nonadjacent Pseudoequivalent Metal Sites in the 38-Atom Trimetallic Close-Packed Framework. *J. Am. Chem. Soc.*, 1999, **121**, 5945-5952.

[53] B. Berti, C. Cesari, C. Femoni, T. Funaioli, M. C. Iapalucci, S. Zacchini, Redox active Ni–Pd carbonyl alloy nanoclusters: syntheses, molecular structures and electrochemistry of $[Ni_{22-x}Pd_{20+x}(CO)_{48}]^{6-}$ (x = 0.62), $[Ni_{29-x}Pd_{6+x}(CO)_{42}]^{6-}$ (x = 0.09) and $[Ni_{29+x}Pd_{6-x}(CO)_{42}]^{6-}$ (x = 0.27). *Dalton Trans.*, 2020, **49**, 5513-5522.

[54] C. Femoni, M. C. Iapalucci, G. Longoni, P. H. Svensson, New high-nuclearity Ni–Pt carbonyl clusters: synthesis and X-ray structure of the ordered $[HNi_{24}Pt_{17}(CO)_{46}]^{5-}$ and the substitutionally Ni/Pt disordered $[Ni_{32}Pt_{24}(CO)_{56}]^{6-}$ cluster anions. *Chem. Commun.*, 2004, 2274-2275.

[55] P. Wix, G. E. Kostakis, V. A. Blatov, D. M. Proserpio, S. P. Perlepes, A. K. Powell, A Database of Topological Representations of Polynuclear Nickel Compounds. *Eur. J. Inorg. Chem.*, 2013, **2013**, 520-526.

[56] D. Fenske, H. Krautscheid, M. Müller, New Intermediate Steps in the Synthesis of Larger Nickel Clusters. *Angew. Chem. Int. Ed.*, 1992, **31**, 321-323.

[57] A. J. Touchton, G. Wu, T. W. Hayton, $[Ni_{23}Se_{12}(PEt_3)_{13}]$ Revisited: Isolation and Characterization of $[Ni_{23}Se_{12}Cl_3(PEt_3)_{10}]$. *Inorg. Chem.*, 2021, **60**, 17586–17592.

[58] J. G. Brennan, T. Siegrist, Y. U. Kwon, S. M. Stuczynski, M. L. Steigerwald, Nickel-selenium-triethylphosphine ($Ni_{23}Se_{12}(PEt_3)_{13}$), an intramolecular intergrowth of nickel selenide (NiSe) and nickel. *J. Am. Chem. Soc.*, 1992, **114**, 10334-10338.

[59] E. R. Jette, F. Foote, Precision Determination of Lattice Constants. *J. Chem. Phys.*, 1935, **3**, 605-616.

[60] Z. Nomikou, B. Schubert, R. Hoffmann, M. L. Steigerwald, Relationships between extended structures and molecular clusters of nickel and tellurium. *Inorg. Chem.*, 1992, **31**, 2201-2209.

[61] T. T. M. Palstra, M. L. Steigerwald, A. P. Ramirez, Y. U. Kwon, S. M. Stuczynski, L. F. Schneemeyer, J. V. Waszczak, J. Zaanen, Electron correlations on a mesoscopic scale: Magnetic properties of transition metal telluride cluster compounds. *Phys. Rev. Lett.*, 1993, **71**, 1768-1771.

[62] T. T. M. Palstra, M. L. Steigerwald, A. P. Ramirez, J. Zaanen, Electron correlations in transition metal-telluride cluster compounds. *Physica B Condens. Matter*, 1994, **199-200**, 619-621.

[63] E. Furet, A. Le Beuze, J.-F. Halet, J.-Y. Saillard, Bonding Analysis in Inorganic Transition-Metal Cubic Clusters. 2. Metal-Centered Hexacapped $M_9(\mu_4\text{-}E)_6L_8$ Species. *J. Am. Chem. Soc.*, 1995, **117**, 4936-4944.

[64] J.-F. Halet, J.-Y. Saillard, in *Structural and Electronic Paradigms in Cluster Chemistry* (Ed.: D. M. P. Mingos), Springer Berlin Heidelberg, Berlin, Heidelberg, **1997**, pp. 81-109.

[65] R. A. Wheeler, Bonding to interstitial main-Group or transition-metal atoms in cubic clusters related to nickel tellurium triethylprophine, $Ni_9(\mu_4\text{-}Te)_6(PEt_3)_8$. *J. Am. Chem. Soc.*, 1990, **112**, 8737-8741.

[66] R. A. Wheeler, Bonding to interstitial main-group or transition-metal atoms in cubic clusters related to nickel tellurium triethylphosphine, $Ni_9(\mu_4\text{-}Te)_6(PEt_3)_8$ [Erratum]. *J. Am. Chem. Soc.*, 1991, **113**, 4046-4046.

[67] A. C. Reber, V. Chauhan, S. N. Khanna, Symmetry and magnetism in Ni_9Te_6 clusters ligated by CO or phosphine ligands. *J. Chem. Phys.*, 2017, **146**, 024302.

[68] X. Roy, C.-H. Lee, A. C. Crowther, C. L. Schenck, T. Besara, R. A. Lalancette, T. Siegrist, P. W. Stephens, L. E. Brus, P. Kim, M. L. Steigerwald, C. Nuckolls, Nanoscale Atoms in Solid-State Chemistry. *Science*, 2013, **341**, 157-160.

[69] C.-H. Lee, L. Liu, C. Bejger, A. Turkiewicz, T. Goko, C. J. Arguello, B. A. Frandsen, S. C. Cheung, T. Medina, T. J. S. Munsie, R. D'Ortenzio, G. M. Luke, T. Besara, R. A. Lalancette, T. Siegrist, P. W. Stephens, A. C. Crowther, L. E. Brus, Y. Matsuo, E. Nakamura, Y. J. Uemura, P. Kim, C. Nuckolls, M. L. Steigerwald, X. Roy, Ferromagnetic Ordering in Superatomic Solids. *J. Am. Chem. Soc.*, 2014, **136**, 16926-16931.

[70] J. P. Zebrowski, R. K. Hayashi, L. F. Dahl, A new family of icosahedral cages with transition metal and main group IV (14) atoms: synthesis and structural-bonding analysis of the $[Ni_{11}(SnR)_2(CO)_{18}]^{2-}$ dianions (R = Bu, Me) containing nickel-centered icosahedral $Ni_{10}Sn_2$ cages and of their unusual $[Ni(SnRCl_2)_4(CO)]^{2-}$ precursors containing a trigonal-bipyramidal d^8 nickel(II) configuration. *J. Am. Chem. Soc.*, 1993, **115**, 1142-1144.

[71] J. P. Zebrowski, R. K. Hayashi, A. Bjarnason, L. F. Dahl, A new family of 14-vertex hexacapped metal cubes with main group IV (14) atoms: synthesis and structural-bonding analysis of $Ni_9(\mu_4\text{-}GeEt)_6(CO)_8$ containing a nickel-centered $Ni_8(\mu_4\text{-}Ge)_6$ cubic cage with an unusual electron count. *J. Am. Chem. Soc.*, 1992, **114**, 3121-3123.

[72] D. Fenske, K. Merzweiler, J. Ohmer, $[Ni_9(\mu_4\text{-}As)_6(PPh_3)_5Cl_3]$, a Cubic Body-centered Ni_9-Cluster. *Angew. Chem. Int. Ed.*, 1988, **27**, 1512-1513.

[73] D. Fenske, C. Persau, Synthesen und Kristallstrukturen von $[Pd_9As_8(PPh_3)_8]$ und $[Pd_9Sb_6(PPh_3)_8]$. *Z. Anorg. Allg. Chem.*, 1991, **593**, 61-68.

[74] P. Pyykkö, Additive Covalent Radii for Single-, Double-, and Triple-Bonded Molecules and Tetrahedrally Bonded Crystals: A Summary. *J. Phys. Chem. A*, 2015, **119**, 2326-2337.

[75] A. J. Kahaian, J. B. Thoden, L. F. Dahl, A new family of metal-centred and noncentred icosahedral cages with transition metal and main group VI atoms: synthesis and structural-bonding analysis of the nickel-centred $[Ni_{11}Se_2(CO)_{18}]^{2-}$, nickel-centred $[Ni_{10}Te_3(CO)_{15}]^{2-}$ and noncentred $[Ni_8Te_4(CO)_{12}]^{2-}$ icosahedral dianions. *J. Chem. Soc., Chem. Commun.*, 1992, 353-355.

[76] A. J. Touchton, G. Wu, T. W. Hayton, Understanding the Early Stages of Nickel Sulfide Nanocluster Growth: Isolation of Ni_3, Ni_4, Ni_5, and Ni_8 Intermediates. *Small*, 2021, **17**, 2003133.

[77] V. G. Albano, F. Demartin, M. C. Iapalucci, F. Laschi, G. Longoni, A. Sironi, P. Zanello, Icosahedral carbonyl clusters $[Ni_{10}Sb_2(\mu_{12}\text{-}Ni)\{Ni(CO)_3\}_2(CO)_{18}]^{n-}$ (n= 2, 3 or 4); synthesis, spectroscopic, electrochemical and bonding analysis. Crystal structures of $[Ni_{10}Sb_2(\mu_{12}\text{-}Ni)\{Ni(CO)_3\}_2(CO)_{18}]^{n-}$ (n= 2 or 3). *J. Chem. Soc., Dalton Trans.*, 1991, 739-748.

[78] V. G. Albano, F. Demartin, M. C. Iapalucci, G. Longoni, A. Sironi, V. Zanotti, Synthesis and X-ray structure of the $[Ni_{13}Sb_2(CO)_{24}]^{n-}$ (n= 2,3,4) cluster anions containing an icosahedral $[Ni_{11}Sb_2(CO)_{18}]^{n-}$ moiety behaving as a distibine ligand and displaying an unexpected electron count. *J. Chem. Soc., Chem. Commun.*, 1990, 547-548.

[79] C. Femoni, M. C. Iapalucci, G. Longoni, S. Zacchini, I. Ciabatti, R. G. Della Valle, M. Mazzani, M. Riccò, The Chemistry of Ni–Sb Carbonyl Clusters – Synthesis and Characterization of the $[Ni_{19}Sb_4(CO)_{26}]^{4-}$ Tetraanion and the Viologen Salts of $[Ni_{13}Sb_2(CO)_{24}]^{n-}$ Carbonyl Clusters. *Eur. J. Inorg. Chem.*, 2014, **2014**, 4151-4158.

[80] V. G. Albano, F. Demartin, M. C. Iapalucci, G. Longoni, M. Monari, P. Zanello, New icosahedral heterometallic nickel carbonyl clusters containing bismuth. *J. Chem. Soc., Dalton Trans.*, 1992, 497-502.

[81] H. N. Kagalwala, E. Gottlieb, G. Li, T. Li, R. Jin, S. Bernhard, Photocatalytic Hydrogen Generation System Using a Nickel-Thiolate Hexameric Cluster. *Inorg. Chem.*, 2013, **52**, 9094-9101.

[82] M. Zhu, S. Zhou, C. Yao, L. Liao, Z. Wu, Reduction-resistant and reduction-catalytic double-crown nickel nanoclusters. *Nanoscale*, 2014, **6**, 14195-14199.

[83] K. S. Joya, L. Sinatra, L. G. AbdulHalim, C. P. Joshi, M. N. Hedhili, O. M. Bakr, I. Hussain, Atomically monodisperse nickel nanoclusters as highly active electrocatalysts for water oxidation. *Nanoscale*, 2016, **8**, 9695-9703.

[84] A. J. Touchton, G. Wu, T. W. Hayton, Generation of a Ni_3 Phosphinidene Cluster from the Ni(0) Synthon, $Ni(\eta^3\text{-}CPh_3)_2$. *Organometallics*, 2020, **39**, 1360-1365.

[85] L. M. Moreau, D.-H. Ha, C. R. Bealing, H. Zhang, R. G. Hennig, R. D. Robinson, Unintended Phosphorus Doping of Nickel Nanoparticles during Synthesis with TOP: A Discovery through Structural Analysis. *Nano Letters*, 2012, **12**, 4530-4539.

[86] H. Zhang, D.-H. Ha, R. Hovden, L. F. Kourkoutis, R. D. Robinson, Controlled Synthesis of Uniform Cobalt Phosphide Hyperbranched Nanocrystals Using Tri-*n*-octylphosphine Oxide as a Phosphorus Source. *Nano Letters*, 2011, **11**, 188-197.

[87] A. J. Touchton, G. Wu, T. W. Hayton, $[Ni_8(CN^tBu)_{12}][Cl]$: A nickel isocyanide nanocluster with a folded nanosheet structure. *J. Chem. Phys.*, 2021, **154**, 211102.

[88] P. Chini, Hexacobalt hexadecacarbonyl and its derivatives. *Chem. Commun.*, 1967, 440-441.

[89] V. Albano, P. Chini, V. Scatturin, Crystal and molecular structures of new cobalt carbonyl clusters. *Chem. Commun.*, 1968, 163-164.

[90] H. Brunner, D. Lucas, T. Monzon, Y. Mugnier, B. Nuber, B. Stubenhofer, A. C. Stückl, J. Wachter, R. Wanninger, M. Zabel, Metal Telluride Clusters Composed of Niobocene Carbonyl, Telluride, and Cobalt Carbonyl Units: Syntheses, Structures, and Reactivity. *Chem. Eur. J.*, 2000, **6**, 493-503.

[91] A. Ebner, J. Wachter, M. Zabel, Synthesis and Characterization of Cobalttelluride Clusters with the Cubic Body-Centered $Co_9Te_6(CO)_8$ Core. *J. Cluster Sci.*, 2004, **15**, 163-174.

[92] J. Wachter, Metal Telluride Clusters — From Small Molecules to Polyhedral Structures. *European Journal of Inorganic Chemistry*, 2004, **2004**, 1367-1378.

[93] M. Bencharif, O. Cador, H. Cattey, A. Ebner, J.-F. Halet, S. Kahlal, W. Meier, Y. Mugnier, J.-Y. Saillard, P. Schwarz, F. Z. Trodi, J. Wachter, M. Zabel, Electron-Sponge Behavior, Reactivity and Electronic Structures of Cobalt-Centered Cubic $Co_9Te_6(CO)_8$ Clusters. *Eur. J. Inorg. Chem.*, 2008, **2008**, 1959-1968.

[94] A. Ebner, W. Meier, Y. Mugnier, J. Wachter, Investigation into the reaction of $(t\text{-}BuC_5H_4)_2Nb(\eta^2\text{-}Te_2)H$ with CH_3Li: Hydride abstraction versus telluride methylation. *Inorg. Chim. Acta*, 2007, **360**, 3330-3334.

[95] A. W. Hull, X-Ray Crystal Analysis of Thirteen Common Metals. *Phys. Rev.*, 1921, **17**, 571-588.

[96] A. W. Cook, G. Wu, T. W. Hayton, A Re-examination of the Synthesis of Monolayer-Protected $Co_x(SCH_2CH_2Ph)_m$ Nanoclusters: Unexpected Formation of a Thiolate-Protected Co(II) T3 Supertetrahedron. *Inorg. Chem.*, 2018, **57**, 8189-8194.

[97] O. Cador, H. Cattey, J.-F. Halet, W. Meier, Y. Mugnier, J. Wachter, J.-Y. Saillard, B. Zouchoune, M. Zabel, Electron-Sponge Behavior and Electronic Structures in Cobalt-Centered Pentagonal Prismatic $Co_{11}Te_7(CO)_{10}$ and $Co_{11}Te_5(CO)_{15}$ Cluster Anions. *Inorg. Chem.*, 2007, **46**, 501-509.

[98] H. Brunner, H. Cattey, W. Meier, Y. Mugnier, A. C. Stückl, J. Wachter, R. Wanninger, M. Zabel, Preparative and Electrochemical Investigations on the Electron Sponge Behavior of Cobalt Telluride Clusters: CO Substitution in $[Co_{11}Te_7(CO)_{10}]^{n-}$ Ions (n=1, 2) by PMe_2Ph and Crystal Structure of $[Co_{11}Te_7(CO)_5(PMe_2Ph)_5]$. *Chem. Eur. J.*, 2003, **9**, 3796-3802.

[99] R. Seidel, R. Kliss, S. Weissgräber, G. Henkel, $[Co_{11}Te_7(CO)_{10}]^{2-}$, a novel cobalt telluride cluster anion containing a body-centred pentagonal-prismatic cobalt framework, and $[Co_4Te_2(CO)_{11}]$, a possible precursor with a metal-deficient pentagonal-planar cobalt frame. *J. Chem. Soc., Chem. Commun.*, 1994, 2791-2792.

[100] K. H. Whitmire, J. R. Eveland, Structural characterization of two large bismuth–cobalt carbonyl clusters: $(PPN)_2[Bi_4Co_9(CO)_8(\mu\text{-}CO)_8]\cdot 2THF$ and $(PPN)_2[Bi_8Co_{14}(CO)_{12}(\mu\text{-}CO)_8]\cdot 1.08THF$. *J. Chem. Soc., Chem. Commun.*, 1994, 1335-1336.

[101] M. Tachikawa, E. L. Muetterties, in *Progress in Inorganic Chemistry*, **1981**, pp. 203-238.

[102] S. C. Lee, W. Lo, R. H. Holm, Developments in the Biomimetic Chemistry of Cubane-Type and Higher Nuclearity Iron–Sulfur Clusters. *Chem. Rev.*, 2014, **114**, 3579-3600.

[103] E. H. Braye, L. F. Dahl, W. Hubel, D. L. Wampler, The Preparation, Properties and Structure of the Iron Carbonyl Carbide $Fe_5(CO)_{15}C$. *J. Am. Chem. Soc.*, 1962, **84**, 4633-4639.

[104] M. R. Churchill, J. Wormald, J. Knight, M. J. Mays, Synthesis and crystallographic characterization of bis(tetramethylammonium) carbidohexadecacarbonylhexaferrate, a hexanuclear carbidocarbonyl derivative of iron. *J. Am. Chem. Soc.*, 1971, **93**, 3073-3074.

[105] M. R. Churchill, J. Wormald, Crystal and molecular structure of tetramethylammonium carbidohexadecacarbonylhexaferrate(2–), $[Me_4N]_2[Fe_6(CO)_{16}C]$, a hexanuclear iron cluster complex with an encapsulated six-co-ordinate carbon atom. *J. Chem. Soc., Dalton Trans.*, 1974, 2410-2415.

[106] P. J. Bailey, B. F. G. Johnson, J. Lewis, The formation of carbides in hexaruthenium carbonyl clusters. *Inorg. Chim. Acta*, 1994, **227**, 197-200.

[107] J. van Wonterghem, S. Mørup, S. W. Charles, S. Wells, J. Villadsen, Formation of a metallic glass by thermal decomposition of $Fe(CO)_5$. *Phys. Rev. Lett.*, 1985, **55**, 410-413.

[108] D. Farrell, S. A. Majetich, J. P. Wilcoxon, Preparation and Characterization of Monodisperse Fe Nanoparticles. *J. Phys. Chem. B*, 2003, **107**, 11022-11030.

[109] G. J. Long, D. Hautot, Q. A. Pankhurst, D. Vandormael, F. Grandjean, J. P. Gaspard, V. Briois, T. Hyeon, K. S. Suslick, Mössbauer-effect and x-ray-absorption spectral study of sonochemically prepared amorphous iron. *Phys. Rev. B*, 1998, **57**, 10716-10722.

[110] M. F. Hansen, P. E. Jönsson, P. Nordblad, P. Svedlindh, Critical dynamics of an interacting magnetic nanoparticle system. *J. Phys. Condens. Matter*, 2002, **14**, 4901-4914.

[111] R. H. Holm, W. Lo, Structural Conversions of Synthetic and Protein-Bound Iron–Sulfur Clusters. *Chem. Rev.*, 2016, **116**, 13685-13713.

[112] A. Eichhöfer, J. Olkowska-Oetzel, D. Fenske, K. Fink, V. Mereacre, A. K. Powell, G. Buth, Synthesis and Structure of an "Iron-Doped" Copper Selenide Cluster Molecule: $[Cu_{30}Fe_2Se_6(SePh)_{24}(dppm)_4]$. *Inorg. Chem.*, 2009, **48**, 8977-8984.

[113] L. Deng, R. H. Holm, Stabilization of Fully Reduced Iron−Sulfur Clusters by Carbene Ligation: The $[Fe_nS_n]^0$ Oxidation Levels (n = 4, 8). *J. Am. Chem. Soc.*, 2008, **130**, 9878-9886.

[114] I. Noda, B. S. Snyder, R. H. Holm, Trichlorotetrakis(triethylphosphine)hexathioheptairon ($Fe_7S_6(PEt_3)_4Cl_3$): a topological link between the prismatic and cube-octahedral structures of iron-sulfur clusters. *Inorg. Chem.*, 1986, **25**, 3851-3853.

[115] B. S. Snyder, M. S. Reynolds, I. Noda, R. H. Holm, Core conversion reactions of iron-sulfur clusters: topological isomer of the Fe_6S_6-prismane core. *Inorg. Chem.*, 1988, **27**, 595-597.

[116] B. S. Synder, R. H. Holm, Hexanuclear iron-sulfur basket clusters: topological isomers of prismanes. Synthesis, structure, and reactions. *Inorg. Chem.*, 1988, **27**, 2339-2347.

[117] S. Rutchick, S. Kim, M. A. Walters, Facile one-step synthesis of tetrachalcogenotetrairon(2+) (chalcogen = sulfur, selenium) cubane-like centers. *Inorg. Chem.*, 1988, **27**, 1513-1515.

[118] G. B. Wong, M. A. Bobrik, R. H. Holm, Inorganic derivatives of iron sulfide thiolate dimers and tetramers: synthesis and properties of the halide series $[Fe_2S_2X_4]^{2-}$ and $[Fe_4S_4X_4]^{2-}$ (X = chlorine, bromine, iodine). *Inorg. Chem.*, 1978, **17**, 578-584.

[119] F. Cecconi, C. A. Ghilardi, S. Midollini, A. Orlandini, Synthesis and crystal structure of the novel paramagnetic selenium/iron stellated octahedral cluster $[Fe_6(\mu_3\text{-}Se)_8(PEt_3)_6][PF_6]$. *Inorg. Chim. Acta*, 1997, **254**, 387-389.

[120] W. Saak, G. Henkel, S. Pohl, A New Route to Iron-Sulfur Clusters: Synthesis and Structure of $[(C_2H_5)_4N]_2Fe_6S_6I_6$. *Angew. Chem. Int. Ed.*, 1984, **23**, 150-151.

[121] R. Wang, W. Xu, J. Zhang, L. Li, A New Hexanuclear Iron−Selenium Nitrosyl Cluster: Primary Exploration of the Preparation Methods, Structure, and Spectroscopic and Electrochemical Properties. *Inorg. Chem.*, 2010, **49**, 4814-4819.

[122] H. Zhang, Z. Ouyang, Y. Liu, Q. Zhang, L. Wang, L. Deng, (Aminocarbene)(Divinyltetramethyldisiloxane)Iron(0) Compounds: A Class of Low-Coordinate Iron(0) Reagents. *Angew. Chem. Int. Ed.*, 2014, **53**, 8432-8436.

[123] T. A. Scott, C. P. Berlinguette, R. H. Holm, H.-C. Zhou, Initial synthesis and structure of an all-ferrous analogue of the fully reduced $[Fe_4S_4]^0$ cluster of the nitrogenase iron protein. *Proc. Natl. Acad. Sci. USA*, 2005, **102**, 9741-9744.

[124] W. L. Jolly, *The Synthesis and Characterization of Inorganic Compounds*, Prentice-Hall, Englewood Cliffs, NJ, 1970.

[125] B. J. Burger, J. E. Bercaw, in *Experimental Organometallic Chemistry, Vol. 357*, American Chemical Society, **1987**, pp. 79-115.

[126] L. Wu, A. Mendoza-Garcia, Q. Li, S. Sun, Organic Phase Syntheses of Magnetic Nanoparticles and Their Applications. *Chem. Rev.*, 2016, **116**, 10473-10512.

[127] S. Sun, Recent Advances in Chemical Synthesis, Self-Assembly, and Applications of FePt Nanoparticles. *Adv. Mater.*, 2006, **18**, 393-403.

[128] R. D. Rutledge, W. H. Morris, M. S. Wellons, Z. Gai, J. Shen, J. Bentley, J. E. Wittig, C. M. Lukehart, Formation of FePt Nanoparticles Having High Coercivity. *J. Am. Chem. Soc.*, 2006, **128**, 14210-14211.

[129] W. S. Seo, J. H. Lee, X. Sun, Y. Suzuki, D. Mann, Z. Liu, M. Terashima, P. C. Yang, M. V. McConnell, D. G. Nishimura, H. Dai, FeCo/graphitic-shell nanocrystals as advanced magnetic-resonance-imaging and near-infrared agents. *Nature Mater.*, 2006, **5**, 971-976.